REPORT DOCUMENTATION PAGE

Form Approved
OMB No. 0704-0188

1. REPORT DATE *(DD-MM-YYYY)*	2. REPORT TYPE	3. DATES COVERED *(From - To)*
08-12-2008	Technical Paper & Briefing Charts	

4. TITLE AND SUBTITLE

Transition Delay in Hypervelocity Boundary Layers by Means of CO_2/Acoustic Instability Interactions (Preprint)

5a. CONTRACT NUMBER

5b. GRANT NUMBER

5c. PROGRAM ELEMENT NUMBER

6. AUTHOR(S)
Ivett A. Leyva (AFRL/RZSA); Stuart Laurence, Amy War-Kei Beierholm, & Hans Hornung (Caltech/Pasadena); Ross Wagnild & Graham Candler (Univ. of Minnesota)

5d. PROJECT NUMBER

5e. TASK NUMBER

5f. WORK UNIT NUMBER
23070725

7. PERFORMING ORGANIZATION NAME(S) AND ADDRESS(ES)

Air Force Research Laboratory (AFMC)
AFRL/RZSA
10 E. Saturn Blvd.
Edwards AFB CA 93524-7680

8. PERFORMING ORGANIZATION REPORT NUMBER

AFRL-RZ-ED-TP-2008-578

9. SPONSORING / MONITORING AGENCY NAME(S) AND ADDRESS(ES)

Air Force Research Laboratory (AFMC)
AFRL/RZS
5 Pollux Drive
Edwards AFB CA 93524-7048

10. SPONSOR/MONITOR'S ACRONYM(S)

11. SPONSOR/MONITOR'S NUMBER(S)
AFRL-RZ-ED-TP-2008-578

12. DISTRIBUTION / AVAILABILITY STATEMENT

Approved for public release; distribution unlimited (PA #08474A).

13. SUPPLEMENTARY NOTES
For presentation at the 47th AIAA Aerospace Sciences Meeting and Exhibit, Orlando, FL, 5-8 January 2009.

14. ABSTRACT

A novel method to delay transition in hypervelocity flows over slender bodies by injecting CO2 into the boundary layer of interest is investigated. The results presented here consist of both experimental and computational data. The experimental data was obtained at Caltech's T5 reflected shock tunnel, while the computational data was obtained at the University of Minnesota. The experimental model was a 5 degree sharp cone, chosen because of its relevance to axisymmetric hypersonic vehicle designs and the wealth of experimental and numerical data available for this geometry. The model was instrumented with thermocouples, providing heat transfer measurements from which transition locations were determined and the efficacy of adding CO2 in delaying transition was gauged. For CO2/N2 freestream blends without injection, the transition Reynolds number more than doubled for mixtures with 40% CO2 mole fraction compared to the case of 100% N2. For the cases with injection, shadowgraph visualizations were obtained, allowing verification of the injection timing. The computations provide encouraging results that for the injection schemes proposed CO2 is reaching high enough temperatures to excite vibrational modes and thus delay transition.

15. SUBJECT TERMS

16. SECURITY CLASSIFICATION OF:			17. LIMITATION OF ABSTRACT	18. NUMBER OF PAGES	19a. NAME OF RESPONSIBLE PERSON
					Dr. Ivett Leyva
a. REPORT	b. ABSTRACT	c. THIS PAGE	SAR	52	19b. TELEPHONE NUMBER *(include area code)*
Unclassified	**Unclassified**	**Unclassified**			N/A

Transition delay in hypervelocity boundary layers by means of CO_2/acoustic instability interactions (Preprint)

Ivett A Leyva[1],
Air Force Research Laboratory, Edwards AFB, Ca, 93536

Stuart Laurence[2], Amy War-Kei Beierholm[3], Hans G. Hornung[4]
Caltech, Pasadena, Ca, 91125

and

Ross Wagnild[5], Graham Candler[6]
University of Minnesota, Minneapolis, Mn, 55455

A novel method to delay transition in hypervelocity flows over slender bodies by injecting CO_2 into the boundary layer of interest is investigated. The results presented here consist of both experimental and computational data. The experimental data was obtained at Caltech's T5 reflected shock tunnel, while the computational data was obtained at the University of Minnesota. The experimental model was a 5 degree sharp cone, chosen because of its relevance to axisymmetric hypersonic vehicle designs and the wealth of experimental and numerical data available for this geometry. The model was instrumented with thermocouples, providing heat transfer measurements from which transition locations were determined and the efficacy of adding CO_2 in delaying transition was gauged. For CO_2/N_2 freestream blends without injection, the transition Reynolds number more than doubled for mixtures with 40% CO_2 mole fraction compared to the case of 100% N_2. For the cases with injection, shadowgraph visualizations were obtained, allowing verification of the injection timing. The computations provide encouraging results that for the injection schemes proposed CO_2 is reaching high enough temperatures to excite vibrational modes and thus delay transition.

Nomenclature

a	=	speed of sound
τ	=	characteristic time of relaxation process
ω	=	angular acoustic frequency
Subscripts		
e	=	equilibrium or boundary layer edge conditions
f	=	frozen

[1] Lead, Combustion Devices Group, AFRL/RZSA, Edwards AFB, CA, AIAA Senior Member.
[2] Postdoctoral Researcher, Caltech, Pasadena, CA.
[3] Former Graduate Student, Caltech, Pasadena, CA now in London, UK.
[4] Professor Emeritus, Caltech, Pasadena, CA, AIAA Fellow.
[5] Graduate Student, University of Minnesota, Minneapolis, MN, AIAA Student Member.
[6] Professor, University of Minnesota, Minneapolis, MN, AIAA Fellow.

I. Introduction

The main justification for this work is the pressing need to reduce aerodynamic heating rates and drag on hypersonic vehicles, for example, the vehicle configurations being studied for a Rocket Based Combined Cycle (RBCC). In a simple approximation, hypersonic aerodynamic heating grows as the cube of the free-stream velocity and linearly with the free-stream density [1]. This, combined with the fact that turbulent heat transfer rates can be an order of magnitude higher than laminar rates for hypersonic Mach numbers [2], result in heating loads becoming a dominant factor in the design of hypersonic vehicles [1]. A reduction in the heating loads allows less thermal protection and hence less weight to carry, or conversely more payload to deliver for a given thrust. While the free-stream velocity may be set for a given application, heating rates and frictional drag can be reduced by keeping the boundary layer laminar for over greater portions of the vehicle body with schemes such as the one proposed here.

A novel method for delaying transition in hypervelocity flows of air by injecting CO_2 into the boundary layer of interest is explained and investigated here. The motivation for this new technique lies in the combination of three relevant findings. The first finding is that, at high Mach numbers, transition occurs through the second (Mack) mode, i.e., amplification of acoustic waves traveling within the boundary layer. The second fact is that molecular vibration and dissociation damp acoustic waves as will be discussed in more detail later in the paper. The third fact is that at relevant conditions for hypersonic flight, CO_2 absorbs energy most strongly at the frequencies most amplified by the Mack mode. Experimental and numerical data show that for a range of about 4-10 MJ/kg, pure CO_2 flows exhibit a significant delay in transition Reynolds number as compared to air and nitrogen flows. Combining these three facts, the idea proposed and investigated here is to inject CO_2 into a boundary layer of interest such that transition can be delayed. Since this is the first time this idea has been put forward, a theoretical, experimental and numerical background is first laid out, then experimental results are presented using CO_2 mixtures in the free stream, without injection, to show the plausibility of the concept. Finally, numerical simulations are presented for proposed injection schemes into the boundary layer.

II. Background

For hypervelocity (both high enthalpy and high Mach number) flows, and especially for highly cooled wall situations, such as those encountered in a reflected-shock tunnel, the dominant transition mechanism is the second or Mack mode [3]. This is an inviscid instability mode associated with wave-like disturbances that become trapped within the boundary layer. This is in contrast to low-speed flows in which the first mode, a viscous mode associated with Tollmien-Schlichting waves [4], is dominant. A decade of research has been carried out in the T5 reflected shock tunnel at Caltech on the effects of vibrational non-equilibrium and dissociation on transition in hypervelocity flows, and is summarized in Hornung et al. [5]. Initial studies focused on transition on a 5-degree sharp cone. The cone was instrumented with thermocouples from which heat flux profiles were obtained and transition locations were determined,. A rapid rise in the heat flux denotes transition. The model was tested in air, N_2, and CO_2, with flow total enthalpies ranging from 3 to 15 MJ/kg. A dramatic transition delay was measured in pure CO_2 flows, as may be observed in Figure 1 (taken from [5]). In this figure, Re^*_{tr} is the transition Reynolds number based on the distance from the cone tip to the transition location. The flow properties are evaluated using the Eckert's reference temperature [6] which has found to be appropriate for discerning trends between different gases at different stagnation enthalpies. Figure 1 shows that the Re^*_{tr} for CO_2 flows is typically about four to five times that of air or N_2 flows of the same flow total enthalpy, h_o. This phenomenon is not observed in low speed flows. These results also point to transition occurring through the second mode, and are thus indicative of nonequilibrium effects playing a role in attenuating the acoustic waves responsible for transition in this mode.

In an effort to understand these findings, Johnson et al. [7] at the University of Minnesota teamed up with the T5 group and performed numerical studies on several of the experimental conditions ran in T5 by Adam and Hornung [8]. Linear stability analyses were carried out in which the transition Re^* in CO_2, air, and N_2 flows were computed under the assumption that the boundary layer transition is caused by the amplification of wave-like disturbances originating in the mean flow (i.e., the second mode). The results of these computations, shown in Figure 2, confirm the experimental observations of Hornung et al. [5]. For the case of air (shot 1162, h_o=9.3 MJ/kg), whether the flow disturbances are reacting or not (this includes both dissociation and vibrational processes) has no impact on the stability of the flow, since, for x>0.106m, disturbances in the boundary layer grow in either case (note that the mean flow is assumed to be reacting irrespective of the assumption made of the disturbances). The experimental data for

this condition showed transition occurring at Re^{*}_{tr}~1e6. However, in the analysis performed in the case of CO_2 (shot 1150, h_o=4MJ/kg), a crucial difference is observed depending on whether the disturbances are assumed to be reacting or nonreacting. In the reacting case, the flow is shown to be stable at all x locations examined and thus no transition is expected over the length of the cone. In contrast, the flow is seen to be unstable if the disturbances are nonreacting. The experimental data for this shot shows almost fully laminar flow, with weak signs of transition towards the end of the cone. Johnson et al. [7] conclude that it is the low dissociation energy of the CO_2 molecule, together with its large number of vibrational modes, that absorb energy from acoustic disturbances in the boundary layer and thus delay transition. It is further noted that, even though transition is a non-linear phenomenon, the frequency of the most amplified disturbance found by a linear analysis is the same as in the non-linear regime. Also, the linear amplification step is the slowest of the steps leading to transition [7]. Therefore, linear analysis can be used to give an order of magnitude prediction on the growth rate and dominant frequencies of the acoustic disturbances in the boundary layer.

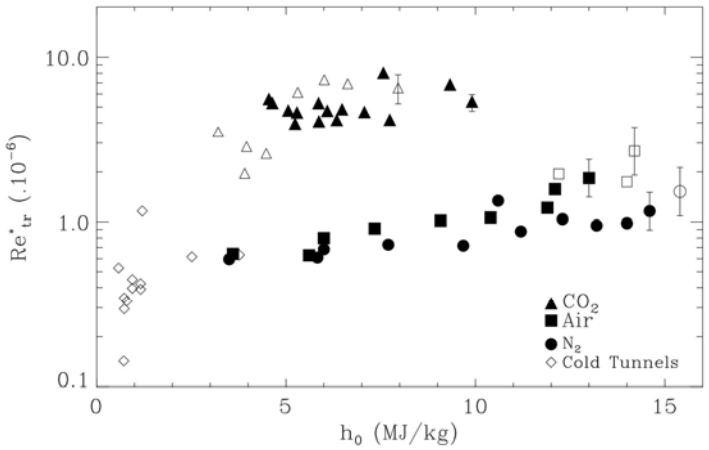

Figure 1. Transition reference Reynolds number for CO_2, Air, and N_2 flows as a function of the flow total enthalpy. The open symbols (non-diamond) are for cases where the flow was laminar to the end of the cone, and thus represent lower bounds. The "Cold Tunnels" data was obtained from independent researchers. Taken from [5].

A few years later, Fujii et al. [9-10] performed a numerical and experimental analysis of the effects of relaxing processes on transition on swept cylinders with sweep angles of 45 and 60 degrees. In this work, the sound absorption rates per wavelength resulting from finite rate relaxation processes are computed for N_2, CO_2, and air at different temperatures. Further details of these computations can be found in Fujii [11]. These computed absorption rates are then compared with the growth rates of wave disturbances in the boundary layer, calculated using an inviscid linear stability analysis based on the work of Reshotko and Beckwith [12], and Mack [3]. The gas is assumed to be perfect in both the mean flow and the disturbances. The results from this analysis are shown in Figure 3 (taken from [10]). In the right plot, showing the case of CO_2, the sound absorption rates (open symbols) are of the same order as the amplification rates for the acoustic disturbances (filled symbols) in the range of frequencies (1-10 MHz) where the acoustic disturbances are most amplified. From this, a significant effect of the relaxation processes on acoustic damping would be expected. It is also worth noting the breadth of the absorption curves, indicating that this damping is effective over a large range of frequencies. In contrast, for the case of air, the sound absorption rates peak at much lower frequencies than those at which the acoustic amplification rates become significant. Thus, no delay in transition due to non-equilibrium processes would be expected in this case. Experimental results were also obtained as part of this study that agree with the predictions of the numerical analysis.

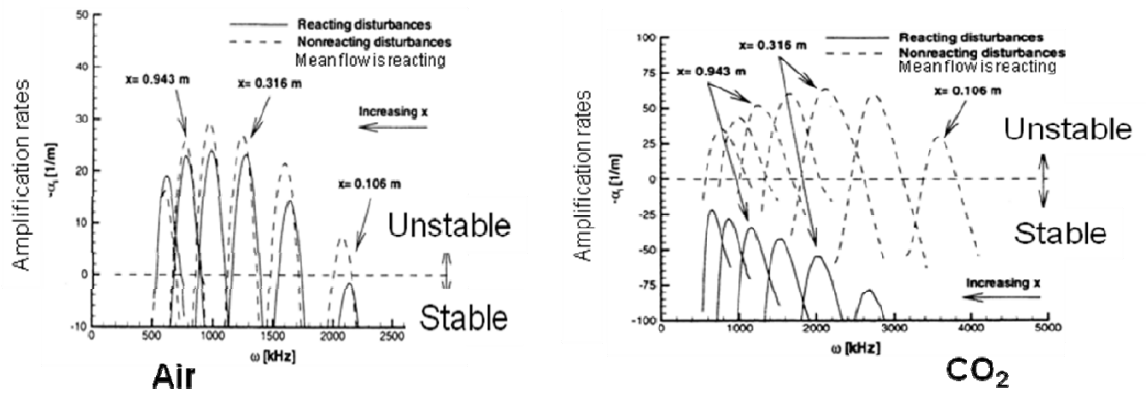

Figure 2. Numerical simulations showing the impact of reacting and nonreacting disturbances on the boundary layer flow stability. Taken from [7]

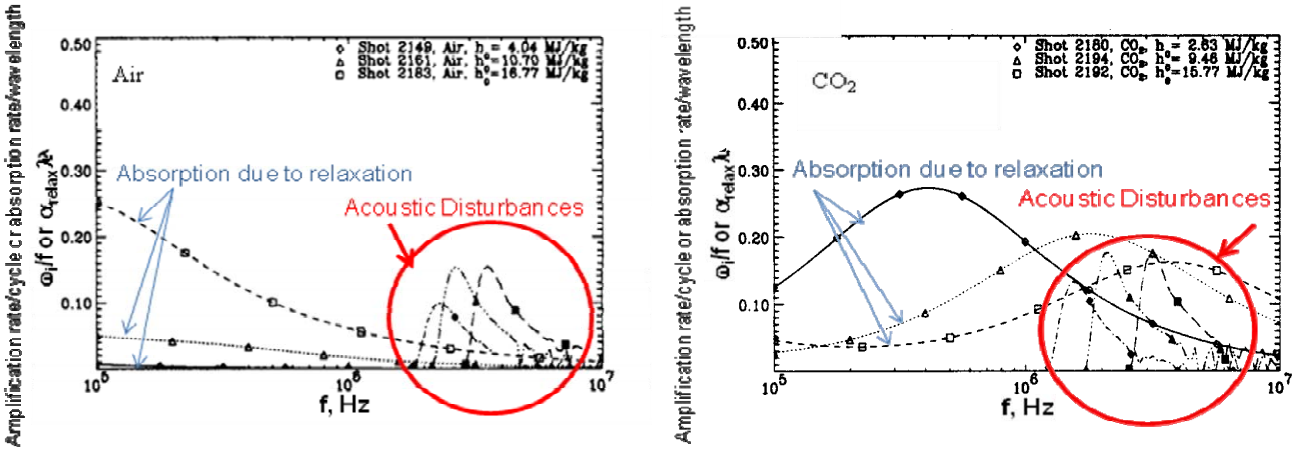

Figure 3. Comparison of absorption rate per wavelength due to relaxation (open symbols) and the amplification rate per cycle (filled symbols) for air and CO_2. The shots refer to particular conditions tested in the T5 facility for a 45-degree swept cylinder. Taken from [10].

The theory of how relaxation processes absorb energy from acoustic disturbances has been known for decades. Lighthill published an extensive article on the subject in 1956 [13], followed by other detailed treatments by Herzfeld and Litovitz [14] in 1959, Clarke and McChesney [15] in 1964 and Vincenti and Kruger [16] in 1967. An intuitive way of understanding this absorption phenomenon is presented in Figure 4. It is assumed here that the gas conditions (temperature and pressure) are close to the characteristic conditions of the given vibration or dissociation process, that the ratio of the frozen to equilibrium speeds of sound is greater than one (i.e., an endothermic reaction), and that the amplitude of the pressure disturbance is small. Examining first the case of a frozen gas, for which the product of the characteristic acoustic disturbance frequency (ω) and the relaxation time (τ) tends to infinity, $\tau\omega\rightarrow\infty$, if an acoustic field ($p'$) is imposed, the variations in density (ρ') will occur along an isentrope (shown as the blue line) characterized by the frozen speed of sound, a_f. Similarly if the gas is in equilibrium ($\tau\omega\rightarrow 0$), the variations in ρ' will happen along a different isentrope (shown as the red line) characterized by the equilibrium speed of sound, a_e. Given the two slopes of the isentropes, one can see that in this case $a_f > a_e$. For these two cases, the variations in p' and ρ' are in phase since they both cross zero at the same time. If the gas is now in nonequilibrium, however, with the acoustic characteristic time of the same order as the relaxation time, $\tau\omega\sim 1$, a different behavior results. For this case, changes in density imposed by changes in pressure don't happen instantly, but rather a number of

collisions are required for the gas to achieve a new value of density. This is represented in the p-ρ diagram as a close curved rather than as a line, indicating the assumption of a limit cycle. As may be seen, the zeros of p' and ρ' now no longer coincide, and a lag is present between the pressure and density changes. The area encompassed by this curve is related to the energy absorbed by the relaxation process in the nonequilibrium gas, which damps the growth of the acoustic waves and thus delays transition. In the situation of interest in the present work, the CO_2 gas injected into the boundary layer is quickly heated to the point where dissociation and/or vibrational nonequilibrium is excited. Then, by the mechanism shown in figure 4, these processes absorb energy from the acoustic waves trapped in the boundary layer. As the CO_2 gas moves along the surface of the cone, it convects this energy away and transfers it to its environment as heat. As heat, this energy does not contribute to transition anymore.

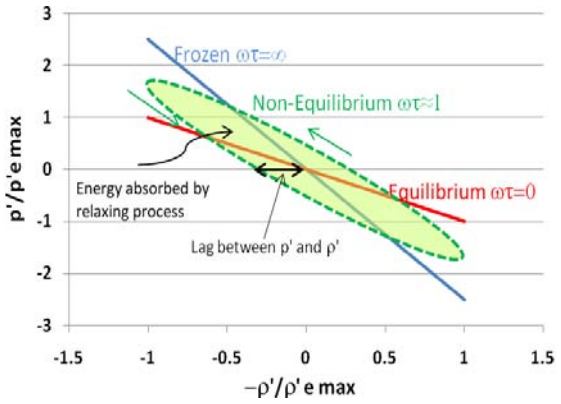

Figure 4. Schematic showing the response of frozen, equilibrium and nonequilibrium gases to small disturbances.

III. Experimental Setup

The facility used in all experiments in the current study was the T5 hypervelocity shock tunnel at the California Institute of Technology. It is the fifth in a series of free-piston driven, reflected shock tunnels built by R.J. Stalker, H.G. Hornung and colleagues [17-18]. The T5 facility consists of four major components: the secondary air reservoir (2R), the compression tube (CT), the shock tube (ST), and the test section/dump tank. The first three of these components are illustrated in Figure 5.

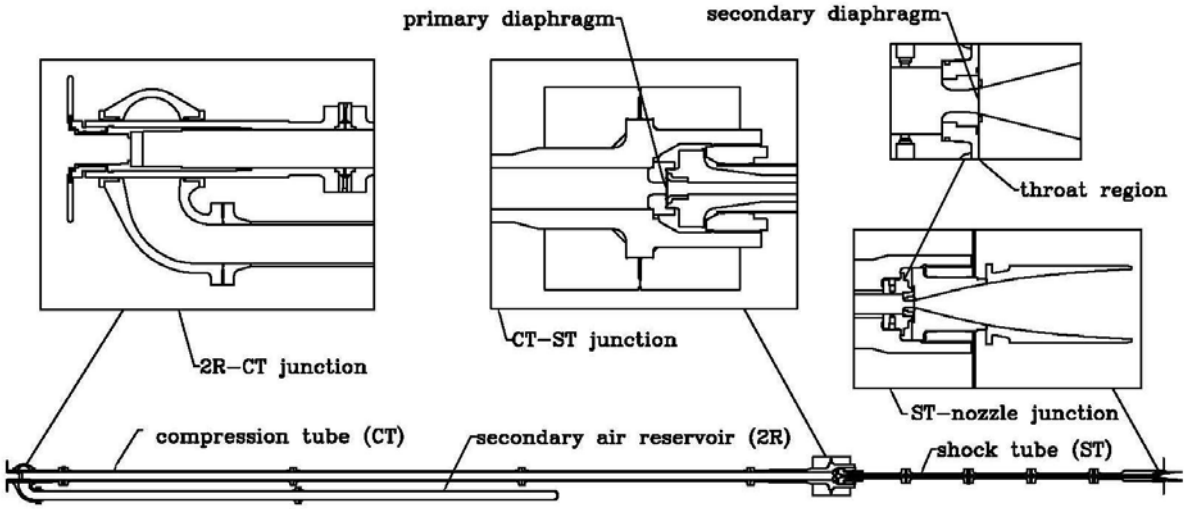

Figure 5: Schematic of the T5 hypervelocity shock tunnel facility.

The test flow is generated by driving a heavy (120 kg) piston down the CT with the release of high-pressure air from the 2R. The CT gas, a mixture of helium and argon, is compressed adiabatically by the advance of the piston until the pressure is sufficiently high to burst the primary diaphragm, located at the junction of the CT and ST. The primary diaphragm typically consists of a 0.187 to 0.270-inch thick stainless steel plate, etched with a X-shaped groove to control the burst pressure. The test gas is initially contained in the ST; the burst of the primary diaphragm produces a shock wave that travels the length of the ST and reflects from the end wall. Stagnation conditions are thus produced at the end of the ST, which then serves as the reservoir for the nozzle expansion. The incident shock also bursts the secondary diaphragm, consisting of a 0.002" mylar membrane located at the ST-nozzle junction. The test gas expands through the nozzle, flowing into the test section and finally into the dump tank. The test section and dump tank are initially evacuated, separated from the ST by the secondary diaphragm. Startup of the flow in the test section typically takes 1ms from the time of arrival of the incident shock at the nozzle throat; the test time is of the order of 1-2 ms. In all experiments in the present series, a contoured nozzle of area ratio 100 was used. The initial pressures in the 2R, CT, and ST were typically 800-1150 psi, 98-116 kPa, and 76-117 kPa, respectively. Test gases were N_2, air, CO_2, and combinations thereof.

The T5 facility is instrumented with various diagnostic tools. Most relevant for the present experiments are the accelerometer attached to the CT, used here to trigger the CO_2 injection, and several pressure transducers along the length of the ST. These transducers are used to measure the incident shock speed and reservoir pressure, from which the flow enthalpy is calculated using the ESTC program [reference], and to trigger the T5 data acquisition system (DAS). The T5 DAS allows simultaneous recording of up to 80 data channels (in addition to the facility data) at a sampling rate of 200 kHz. The T5 optical setup is a typical Z-arrangement Schlieren system, capable of recording either a single frame or a sequence of high-speed images during the test period.

The model employed in the current experiments was the slender cone used in a number of previous experimental studies in T5, including that of Adam [8]. It is a 5 degree half-angle cone of approximately 1m in length and is composed of three sections: a sharp tip fabricated of molybdenum (to withstand the high heat fluxes), a mid-section, and the main body instrumented with 21 thermocouples. This shape was chosen because of the wealth of experimental and numerical data available, which will be used for comparison with the results from this program. A photograph of the cone model is shown in Figure 6.

Figure 6. Cone model used for all experiments in this study. The solid mid-section, used in most experiments, has here been replaced by an injection tip.

IV. Experimental Results

A. Freestream blends

In initial experiments, mixtures of N_2 and CO_2 in various ratios were used as the test gas, with no injection. These runs serve as a baseline, assessing the effect of the presence of CO_2 in the boundary layer independent of any injection scheme. The average p_0 for these runs was 51MPa and the average mixture h_0 was 10.7 MJ/kg; the run conditions are given in the Appendix. The transition location for each shot was deduced from the heat transfer profile obtained along the length of the cone. Figure 7 shows a typical heat flux profile, plotted as the Stanton number versus the Reynolds number based on the thermocouple location and edge conditions. Lines corresponding to both laminar and turbulent theoretical (or semi-empirical) predictions are also shown. In the turbulent case, two of the more successful models are shown; details of the calculation of these three lines may be found in White [reference]. In the case shown, the beginning of transition from laminar to turbulent flow in the boundary layer is seen. Good agreement between the initial experimental data points and the theoretical laminar prediction shows that the flow is initially laminar. Then, as the Re increases, a sharp increase in the heat flux is seen. The intersection between the laminar prediction line and a least-squares fit to these data can be used as a good approximation to the onset of transition. From this intersection, the transition Reynolds number, $Re_{tr} = \rho_e U_e x_{tr}/\mu_e$, can be determined. As mentioned in the introduction of this paper, the transitional/turbulent heat flux values are significantly higher than those in the laminar regime, illustrating the potential value of suppressing such transition on a vehicle body.

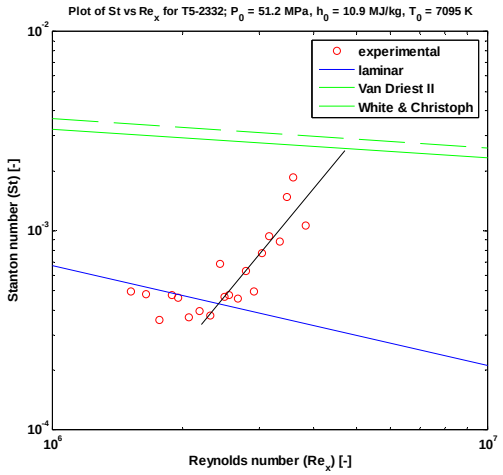

Figure 7. Normalized heat transfer profile for a free-stream mixture of 95% N_2 /5% CO_2 by mole fraction.

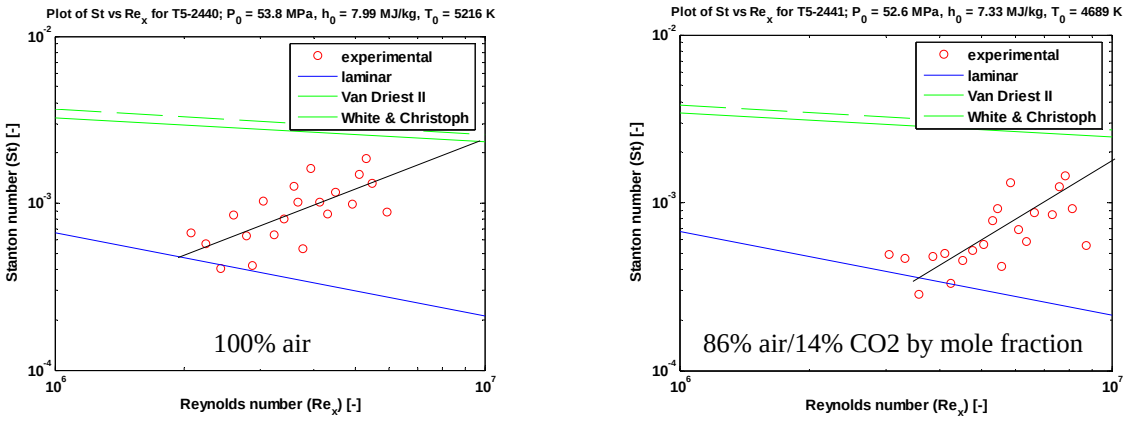

Figure 8. Normalized heat transfer profile for free-stream mixtures of air and CO_2

Additional shots were run with mixtures of CO_2 and air, the results from which are shown in Figure 8. As with N_2/CO_2 mixtures, the transition Reynolds number is seen to move noticeably to the right when CO_2 is added to the air test gas, even though it is only 14% by mole faction. In figure 9, the transition data collected for CO_2 mixtures with both N_2 and air is plotted together. For this data, a switch has been made from the Reynolds number based on the edge conditions to $Re^*_{tr} = \rho^* U_e x_{tr}/\mu^*$ where the density and viscosity are evaluated at the conditions corresponding to Eckert's reference temperature, denoted by the * superscript . As mentioned in the background section, the use of such conditions is more appropriate for discerning trends between different gases at different stagnation enthalpies. As might be expected, the minimum value of Re^*_{tr} occurs for 100% N_2 or air , but, as CO_2 is added, Re^*_{tr} increases significantly. In the case of N_2, it has more than doubled by the time the CO_2 fraction reaches 40%. In the case of air, Re^*_{tr} also increases significantly if the mole fraction of CO_2 is increased to 14%, but there are insufficient data points for quantitative conclusions to be drawn. The data pertaining to 100% CO_2 was inconclusive regarding the transition location: although suggestions of transition appear toward the end of the cone, there was not a clear trend. The data point plotted here thus signifies the minimum value that Re^*_{tr} could take, corresponding to the position of the last thermocouple. Previous experiments have shown Re^*_{tr} to be significantly higher in pure CO_2 flows than in either air or pure N_2 flows at the same enthalpy. This is the first time, however, that experiments have been performed in T5 that have shown CO_2 to be effective in delaying transition when present as a component of the free-stream gas. This result lends optimism to the efficacy of the transition delay technique being investigated here.

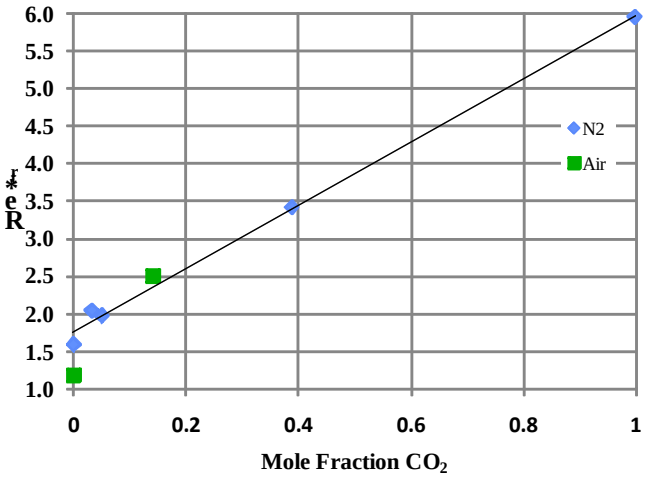

Figure 9. The effect of CO_2 mole fraction in the test gas on Re^*_{tr} for flows over a 5 degree sharp cone, for a free-stream otherwise consisting of N_2 or air.

B. Injection Scheme

Several injector tip geometries were designed and built for this experimental series. A schematic of the initial design is shown in Figure 10; the CFD simulations discussed in the following section are based on this geometry. The CO_2 flows from a high-pressure run tank outside the test section, through a series of pipes into a reservoir in the tip, then exits to the surface of the cone through a series of holes. Only qualitative experimental data was able to be obtained with CO_2 injection since the instrumentation on the cone failed midway through testing (after about 10 years of use). However, based on this qualitative data and visualizations of the injected flow, it was decided to build a new injector tip for the next set of experiments. The new injector has twice as many holes and approximately double the flow area of the previous tip. This will allow lower injection pressures to be used for the same mass flow rate. A new cone model has also been constructed with 80 thermocouples uniformly distributed in the circumferential and axial directions. This will allow more precise determination of the transition location in comparison to the older model, which was restricted to 21 thermocouples located on only one side of the cone.

One of the principal engineering challenges of this project has been ensuring that the injected flow is adequately established by the time of arrival of the main flow in the test section, as there is only ~180ms from the earliest signal generated by the facility to the beginning of the test period. Through visualizations of the injected flow into ambient air, and comparisons of the run tank pressure traces with those obtained during experiments, it has been verified that the injected gas first arrives at the cone surface after ~70ms, and that injection is well established by the beginning of the test time (see Figure 10 B&C).

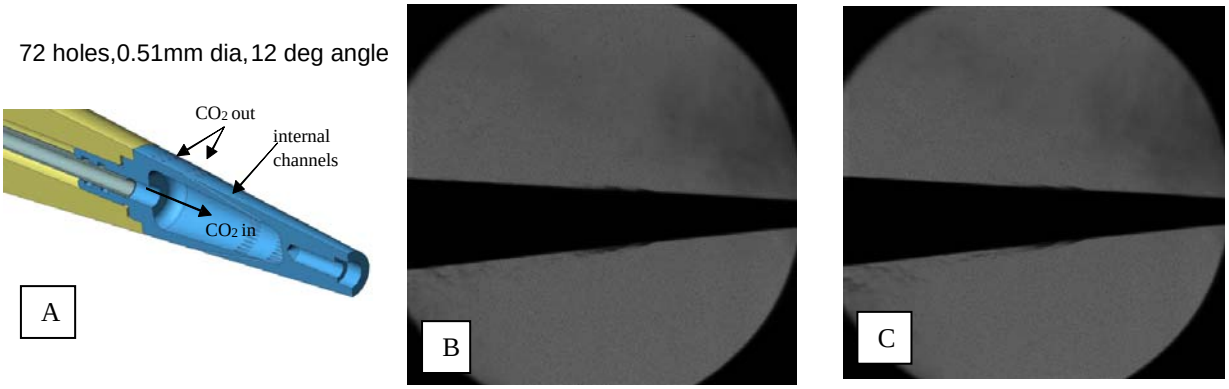

Figure 10. A. Schematic of CO_2 injection section. Flow visualization of CO_2 injection from injector tip into ambient air. B: flow at 73 ms after trigger. C: flow at 78 ms after trigger.

V. Computational Results

Three injection cases were performed on a 5 degree cone with a single row of injector ports. This is a simplified version of the actual tip used in the experiments. Each case had a different injection pressure in order to study the effect this has on the flow in the shock and boundary layers and the CO_2 distribution. All cases were run with the same freestream conditions. These conditions, as well as the injection pressures, are listed in table 2 of the appendix. A case without injection was also performed to evaluate the effect the injection has on the boundary layer height and also to quantify the improvement in stability.

A. CFD Solvers

For these simulations, a finite volume formulation was used to solve the compressible Navier-Stokes equations. In the no-injection case, the structured solver DPLR was run on a two dimensional grid with an axi-symmetric formulation [19]. In the injection cases, a hybrid, unstructured solver [20] was used on a ten degree slice of the test body. In both cases, the inviscid fluxes were evaluated using a second-order accurate, modified Steger-Warming flux vector splitting method. For the viscous fluxes, gradient reconstruction was accomplished by using a weighted least-squares method. The time integration was a first-order accurate, implicit method. The implicit method is implemented in two different ways depending on the location in the grid. In the near-wall region, where the grid is clustered to the wall, the implicit method used was line relaxation, with lines being solved in the wall-normal direction. Where lines are not generated, a full matrix point relaxation was used. Both codes were run in parallel using MPI.

B. Gas Properties

For these simulations, nine chemical species were used: CO_2, CO, N_2, O_2, NO, CN, C, N, and O. The viscosity for each species was calculated using the high temperature Blottner fits and the mixture viscosity was calculated using Wilke's semi-empirical mixing law. A Landau-Teller vibrational relaxation model was used for the translational-vibrational energy exchange with the jet-on cases using the characteristic relaxation times based on the Milliken and White semi-empirical curve fits [22-24]. The chemical reactions modeled in these simulations are:

$$CO_2 + M \Leftrightarrow CO + O + M \quad (1)$$

$$CO + M \Leftrightarrow C + O + M \quad (2)$$

$$N_2 + M \Leftrightarrow N + N + M \quad (3)$$

$$O_2 + M \Leftrightarrow O + O + M \quad (4)$$

$$NO + M \Leftrightarrow N + O + M \quad (5)$$

$$CN + M \Leftrightarrow C + N + M \quad (6)$$

$$N_2 + O \Leftrightarrow NO + N \quad (7)$$

$$O_2 + N \Leftrightarrow NO + O \quad (8)$$

$$CO + O \Leftrightarrow O_2 + C \quad (9)$$

$$CO_2 + O \Leftrightarrow O_2 + CO \quad (10)$$

$$CO + N \Leftrightarrow CN + O \quad (11)$$

$$N_2 + C \Leftrightarrow CN + N \quad (12)$$

$$CN + O \Leftrightarrow NO + N \quad (13)$$

The forward reaction rate coefficients are taken from Park et al. [22], except for reactions seven and eight, which are from Bose and Candler [24, 25]. The equilibrium coefficients are taken from Park [27], except for reactions one, two, and ten, which are generated from fitting the data given in McBride et al. [28].

C. **Grid Generation**

For the two dimensional, axi-symmetric case, a structured grid of quadrilateral elements was used. The grid was generated using a module in software suite STABL [29]. The three dimensional grid was composed of an unstructured set of hexahedral and triangular prism cells. It was generated using a combination of the commercial grid generation software packages Gridpro and Gridgen.

Only one of the injector ports was modeled to reduce the computation cost of the problem, resulting in a ten degree slice of the full test body. The topology around the port was designed to provide a continuous layer of cells normal to wall, in order to take advantage of the line relaxation method. An area of high cell density in the streamwise direction as well as a layer of cells were nested around the port to add additional refinement in order to capture the complexity of the flow in this region. This portion of the grid, created using gridpro, can be seen in Figure 11.

This grid was imported into Gridgen to create a mesh on the rest of the cone. At the nose, an initial cell spacing in the streamwise direction of approximately 0.23 μm was used in order to resolve the sharp gradients at the nose. The sharp nose was approximated with hexahedral cells. It was found that using triangular prism cells at the nose created a significant amount of error for the isothermal wall condition. Due to the axisymmetric nature of flow before the injector port, only two cells were used in the spanwise direction to reduce the computational cost. A short distance before the injector port, the number of spanwise cells was increased from two to forty, by means of triangular prism cells, in order to resolve the shape of the port as well as the complexity of the flow in this region. Also, the streamwise cell spacing in the regions outside of the port had a sparser cell density, however the cell stretching maintained continuity through the use of a hyperbolic tangent distribution. The total number of cells for the grid was approximately 2.2 million cells.

Another requirement for an injection flow is to model the plenum chamber. It has been shown [30] that to correctly model the mass and momentum flux out of the port that both a subsonic, plenum condition must be applied and any geometry that could reduce the discharge coefficient must be modeled. For the jet-on case, a slightly modified version of the plenum chamber was modeled. This shape is displayed in Figure 11.

The clustering near the wall allowed for an initial cell spacing of less than one viscous wall unit for the entire cone surface. This was not the case inside the injector port near the plenum, where the value was on the order of one wall unit. However, due to the small velocities in this region, the effect on the flow field is not significant.

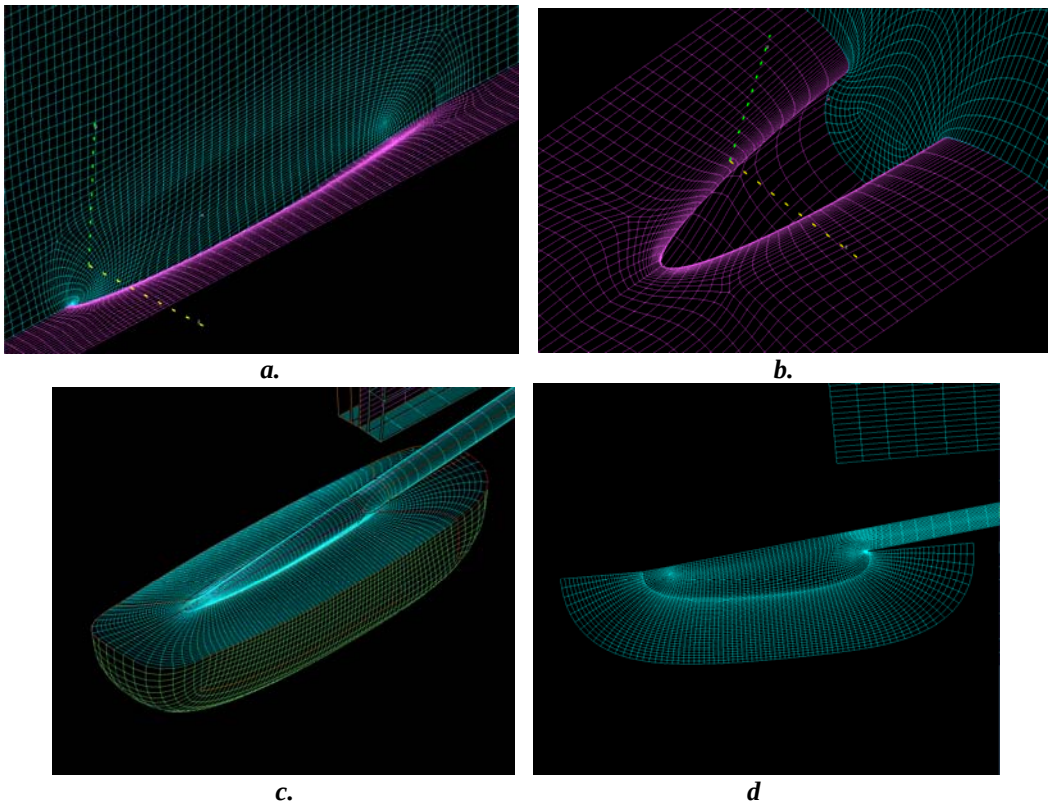

Figure 11. The grid geometry. Pictures a and b are views of the injector port on the surface of the cone. Pictures c and d are views of the plenum chamber. These views were taken before clustering was applied to the grid.

D. Results

A prototypical contour plot of Mach number at the location of injection is seen in figure 12. The surface of the cone is colored in gray and the black lines are fluid streamlines. In all cases tested, the pressure in the reservoir causes the injection gas to reach sonic speed near the exit of the injector port. This provides the injection gas with enough momentum to displace the boundary layer and penetrate into the shock layer. A higher injection pressure results in a larger height of penetration. This action results in a shock that develops in front of the injection stream and is transmitted to the oblique shock off the nose of the cone, causing the oblique shock to change its angle to the surface. Due to the displacement of the shock layer, the fluid that encounters the injection stream rolls off on each side of it as seen in some of the streamlines drawn in figure 12. When paired with the wall-normal momentum of the injection stream, it causes a vortex to form near the wall at the front of the injector port, which wraps around both sides of the injection stream. These vortices play a major role in the distribution of the injection gas downstream. Secondly, they aid in heating the cell of cold injection gas.

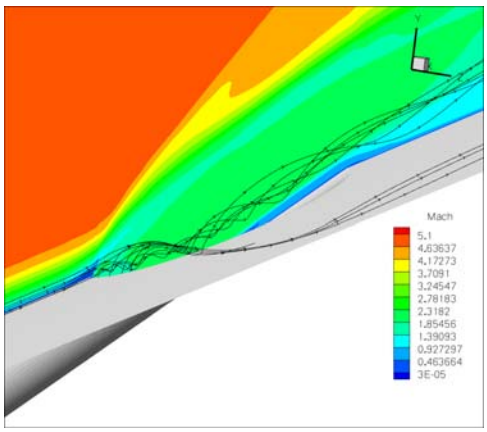

Figure 12. Mach contours of the gas injection. The cone surface is colored in gray and the black lines represent fluid streamlines. This image was taken from the data obtained in case 3.

Downstream of the injection, the core of injection gas starts mixing in the spanwise direction, due to both diffusion and convection. For case 1 with the lowest injection pressure (32.2 psia), at a distance of 30 cm from the nose of the cone, there is CO_2 present over the whole surface of the cone, as seen in figure 13. From the plot of temperature contours, it can be seen that CO_2 is being heated by the higher temperature fluid that sits on top of the CO_2. At this location, a large portion of the CO_2 has reached a temperature of approximately 2000 K. The data shows that the vibrational temperature is approximately equal to the translational temperature. This temperature is high enough to allow activation of three of the four vibrational modes of CO_2. As previously stated, this is beneficial to the stability of the boundary layer. The boundary layer edge is approximately 1.2 mm. At this location in the no-injection case, the boundary layer edge is about 0.8 mm thick, implying that the injection of CO_2 has made the boundary layer grow.

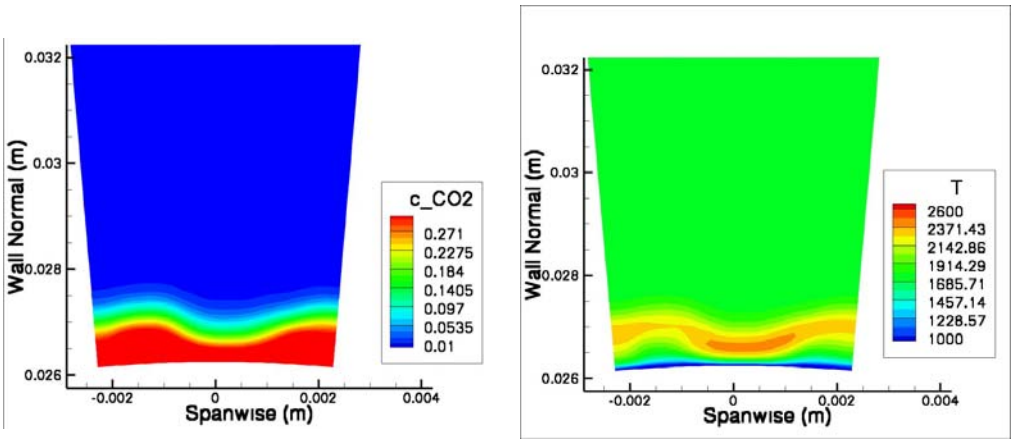

Figure 13. Concentration and Temperatures profiles at 30 cm from the cone tip. These images are taken from case 1

Further down the cone, the distribution of CO_2 has smoothed out and it has become a smaller constituent of the mixture, as seen in figure 14. However, areas exist where the mass fraction is above 10%, which is a large enough percentage to allow for increased stability, as inferred from figure 9. Looking at the temperature contours, a large portion of the CO_2 is now being heated to approximately 2200 K, which brings it within range of starting to dissociate. As stated in the discussion of figure 4, this can be advantageous due to ability of the dissociation to absorb energy of disturbances in the boundary layer. Also important to note, the height of the boundary layer at this location is approximately 1.3 mm. This is relatively larger than the no-injection case, which has a boundary layer height of approximately 1.05 mm.

Profiles such as those in figures 13 and 14 are seen in the other two cases tested, with the only difference being the amount of CO_2 in the boundary layer and the height of the high temperature zone. This is to be expected from adding more mass and more wall normal momentum into the boundary layer, however minimizing this effect is one of the goals of the project. It would seem that the low pressure case (case 1) would have the advantage over the higher pressure cases in that CO_2 is successfully added to the full surface of the cone with the smallest impact on the boundary layer.

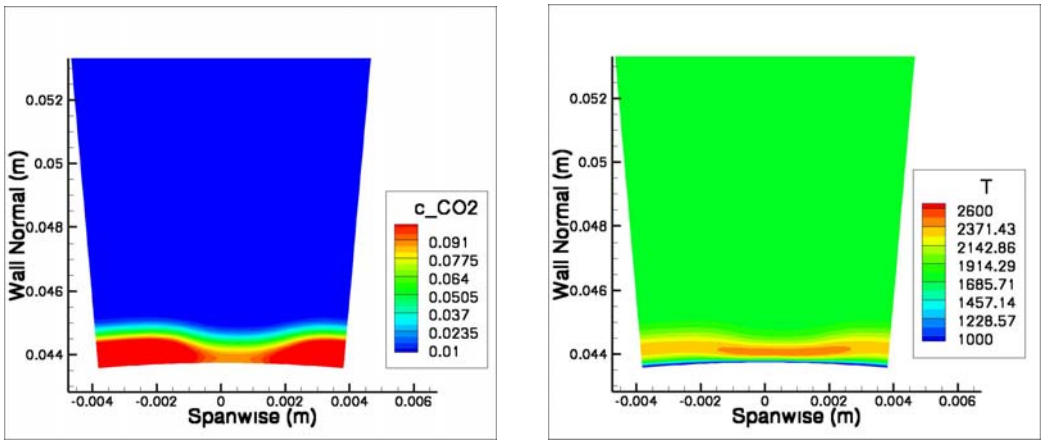

Figure 14. Concentration and Temperatures profiles at 50 cm from the cone tip. This images are taken from case 1.

It is important to note that injecting CO_2 with a single row of injectors may not be the best suited to achieve the goal of an even distribution of CO_2 over the cone's surface. This is best demonstrated by the wavy distribution of CO_2 as seen in figure 13. A possible solution to this is to use the model seen in figure 10. With two rows of offset injector ports, the second row could fill in the gaps in the distribution caused by the flow field of the first row. Simulations of this method of injection will be run in the future to confirm this.

VI. Conclusion

In this project, a new technique to delay the transition in hypervelocity flows by injecting CO_2 into the boundary layer of interest has been proposed and investigated. A series of experiments have been conducted at Caltech's T5 to test this technique in high enthalpy flows over a 5 degree sharp cone. This geometry was chosen due to its relevance to axisymmetric vehicle configurations and to the wealth of previous data available for comparison with the obtained Re*tr data. Initial experiments used mixtures of CO_2/N_2 as the test gas, rather than introducing CO_2 directly to the boundary layer of the cone. The obtained results demonstrate that the addition of CO_2 delays the onset of transition. For example, in the case of $60\%N_2/40\%CO_2$ by mole fraction, the value of Re*tr was more than double that of the case of 100% N_2. A similar effect was noted in experiments using mixtures of air and CO_2 as the test gas. A small number of experiments were subsequently carried out with CO_2 injection into an air freestream, but questionable thermocouple readings meant that no quantitative conclusions could be drawn from these. However, tests were carried out in which the injected flow was visualized, providing confirmation that the triggering of the injection system is appropriately timed to provide adequate injected CO_2 during the test time. In fact, the CO_2 flow starts approximately 100ms before the main flow arrives, providing enough time for the injection flow to be fully established. This injection timing system will be used in upcoming experiments.

A series of numerical simulations were also completed with comparable freestream conditions to those attained in T5and a simplified injection geometry based on the actual cone tip built. From the numerical results, it was found that the CO_2 reaches a temperature of about 2000K after 30 cm from the cone tip. This is encouraging since the lowest vibrational characteristic temperature for this gas is 960K. Also, the mass fraction contours of CO_2 showed that it is being rapidly mixed along the lateral direction of the cone, which is desired. The CFD results for the

different reservoir pressures show that the lowest pressure tried (32 psia) might be most suitable as a start point for the next series of experiments since this shows the least disruption to the boundary layer.

Appendix

Table 1. Run Conditions

Shot No.	P_0 (MPa)	T_0 (K)	h_0 (MJ/kg)	$[N_2]$ or [air] (mol/mol)	$[CO_2]$ (mol/mol)
2331	52.2	7375	10.75	1.00 N2	0.00
2332	51.2	7095	10.90	0.95 N2	0.05
2333	50.0	4434	9.43	0.00 N2	1.00
2334	50.1	5380	10.89	0.61 N2	0.39
2337	51.2	7379	11.37	0.97 N2	0.03
2440	7.99	53.8	5216	1.00 air	0.00
2441	52.6	4689	7.33	0.86 air	0.14

Table 2. Conditions used for CFD simulations

Stagnation Conditions		Freestream Conditions	
Pressure (MPa)	58.5	Density kg/m^3	0.06032
Temperature (K)	6305.3	Temperature (K)	1564
Enthalpy (MJ/kg)	10.47	Velocity (m/s)	4080
		Wall Temperature (K)	293
		Minf	5.1

Gas Composition (by mass fraction)	
N2	0.7345
O2	0.1844
NO	0.0654
N	0.0
O	0.0157

All at 300 K	Case 1	Case 2	Case 3
Pressure (psia)	32.2	64.4	107
Mass Flux (g/s)/hole	0.213	0.438	0.746

Acknowledgments

The authors would like to thank Bahram Valiferdowsi for helping with the design of the injection pieces and with the maintenance of the facility. Financial support for this work was provided in part by the Air Force Office of Scientific Research, USAF, under grant/contract number F49620-IHOUSE07E0000. The program manager is Dr. John Schmisseur to whom the authors are grateful for his continued support throughout this project.

References

1 Anderson Jr., J.D., *Hypersonic and High Temperature Gas Dynamics*, McGraw-Hill 1989.
2 Heisner, W.H., Pratt, D.T., "*Hypersonic Airbreathing Propulsion*," AIAA Education Series, 1994.
3 Mack, L.M., "Boundary-layer stability theory," In Special Course on Stability and Transition of Laminar Flow, AGARD Report Number 709, 1984.
4 Schlichting, H., Boundary Layer Theory. McGraw-Hill Company, 1987.
5 Hornung, H.G., Adam, P.H., Germain, P., Fujii, K., Rasheed, A., "On transition and transition control in hypervelocity flows," Proceedings of the Ninth Asian Congress of Fluid Mechanics
6 Eckert, E.R.G., "Engineering relations for friction and heat transfer to surfaces in high velocity flow," Journal of the Aeronautical Sciences, 22:585-587, Aug. 1955.
7 Johnson, H.B., Seipp, T.G., Candler, G.V., "Numerical study of hypersonic reacting boundary layer transition on cones," Physics of Fluids, 10 (10): 2676-2685 Oct. 1998.
8 Adam P.H. and Hornung, H.G., ''Enthalpy effects on hypervelocity boundary-layer transition: Ground test and flight data,'' J. Spacecraft and Rockets 34, 614 (1997).
9 Fujii, K., Hornung, H.G., "An experiment of high-enthalpy effect on attachment line transition," AIAA 2001-2779, 2001.
10 Fujii, K., Hornung, H.G., "Experimental investigation of high-enthalpy effects on attachment-line boundary layer transition," AIAA Journal, Vol. 41, No. 7, July 2003.
11 Fujii, K., Hornung, H.G., "A Procedure to Estimate the Absorption Rate of Sound Propagating Through High Temperature Gas", GALCIT Report FM 2001.004, August 8, 2001.
12 Reshotko, E., Beckwith, I.E., "Compressible laminar boundary layer over a yawed infinite cylinder with heat transfer and arbitrary Prandtl number," Technical Report NACA Report 1379, National Advisory Committee for Aeronautics (NACA), 1958.
13 Lighthill, M.J., Viscosity effects in sound waves of finite amplitude. In G.K. Batchelor and R.M. Davies, editors, Surveys in Mechanics, pages 250-351. Cambridge University Press, 1956.
14 Herzfeld, K.F., and Litovitz T.A., Absorption and Dispersion of Ultrasonic Waves, New York, Academic Press 1959.
15 Clarke J.F. and McChesney M., The Dynamics of Real Gases. Butterworths, 1964.
16 Vincenti W.G. and Kruger C.H.. Introduction to Physical Gas Dynamics. Krieger Publishing Company, 1965.
17 Hornung, H., Belanger, J., "Role and techniques of ground testing simulation of flows up to orbital speeds", AIAA 90-1377.
18 Hornung, H., "Performance data of the new free-piston shock tunnel at GALCIT", AIAA 92-3943.
19 Vatistas, G. H., Lin, S., and Kwok, C. K., "Reverse Flow Radius in Vortex Chambers," AIAA Journal, Vol. 24, No. 11, 1986, pp. 1872, 1873.
20 Wright, M. J., Candler, G. V., and Bose, D. "A Data-Parallel Line-Relaxation Method for the Navier-Stokes Equations," Paper 97-2046CP, AIAA, June 1997.
21 Nompelis, I., Drayna, T., Candler, G. V., "Development of a Hybrid Unstructured Implicit Solver for the Simulation of Reacting Flow over Complex Geometries," AIAA Paper No. 2004-2227, June 2004.
22 Park, C., "Review of Chemical-Kinetic Problems of Future NASA Missions, I: Earth Entries," Journal of Thermophysics and Heat Transfer, Vol. 7, No. 3, 1993, pp. 385-398.

23 Park, C., Howe, J.T., Jaffe, R.J., and Candler, G.V., "Review of Chemical-Kinetic Problems of Future NASA Missions, I: Mars Entries," Journal of Thermophysics and Heat Transfer, Vol. 8, No. 1, 1994, pp. 9-23.
24 Camac, M., "CO2 Relaxation Processes in Shock Waves," Fundamental Phenomena in Hypersonic Flow, Ed. J.G. Hall, Cornell University Press, pp. 195-215, 1964.
25 Bose, D. and Candler, G. V. "Thermal Rate Constants of the N2 + O -> NO + N Reaction Using Ab Initio 3a" and 3a' Potential Energy Surfaces," Journal of Chemical Physics, vol. 104, No. 8, pp. 2825-2833, 1996.
26 Bose, D. and Candler, G. V. "Thermal Rate Constants of the O2 + N -> NO + O Reaction Based on the 2a' and 4a' Potential Energy Surfaces," Journal of Chemical Physics, vol. 107, No. 16, pp. 6136-6145, 1997.
27 Park, C., Nonequilibrium Hypersonic Aerodynamics, Wiley, 1990
28 McBride, B. J., Zehe, M. J., and Gordon, S. "NASA Glenn Coefficients for Calculating Thermodynamic Properties of Individual Species," Tech. Rep. 2002-211556, NASA, September 2002.
29 Johnson, H. B., Seipp, T. G., and Candler, G. V., "Numerical Study of Hypersonic Reacting Boundary Layer Transition on Cones," Physics of Fluids, vol. 10, October 1998.
30 Peterson, D. M., Subbareddy, P., and Candler, G. V., "Detached Eddy Simulations of Flush Wall Injection into a Supersonic Freestream," 42nd AIAA/ASME/SAE/ASEE Joint Propulsion Conference and Exhibit, Sacramento, CA, July 9-12, 2006, AIAA Paper No. 2006-4576.

GALCIT
Caltech

Transition delay in hypervelocity boundary layers by means of CO_2/acoustics interactions

Dr. Ivett A. Leyva
AFRL/RZSA
Edwards AFB, Ca.

Dr. Stuart Laurence, Amy Kar-Wei Beierholm, Prof. Hans Hornung

GALCIT, Caltech, Pasadena, CA

AFOSR Grant F49620-IHOUSE07E0000

Ross Wagnild, Prof. Graham Candler

University of Minnesota, Minneapolis, MN

AIAA Aerospace Science Meeting
Orlando, Fl
January 5-8, 2009

Delay transition using non-equilibrium CO_2

GALCIT
Caltech

PROBLEM: **In hypersonic flight, heating loads are typically a dominant design factor**

Turbulent heat transfer rates can be about an order of magnitude higher than laminar rates at hypersonic Mach numbers

A reduction in heating loads by keeping the boundary layer laminar longer means less thermal protection needed and hence less weight to carry, or conversely more payload deliverable for a given thrust.

OBJECTIVE: Delay transition from laminar to turbulent flow in the boundary layer of a slender hypersonic body by using nonequilibrium CO_2

Transition in high Mach numbers occurs through the Mack mode – amplification of acoustic waves traveling in the boundary layer

Molecular vibration and dissociation damp acoustic waves

At relevant conditions, CO_2 absorbs most energy at the frequencies most strongly amplified by 2nd (Mack) mode

Inject CO_2 to delay transition in air flows of interest

Background

GALCIT
Caltech

- **Experimental data shows that transition is delayed for CO_2 flows compared with N_2 and air flows for a given stagnation enthalpy, h_o**
- **These observations point to a second mode transition (or Mack mode) for the conditions studied as well as to the importance of nonequilibrium effects of CO_2 on stabilizing the flow**

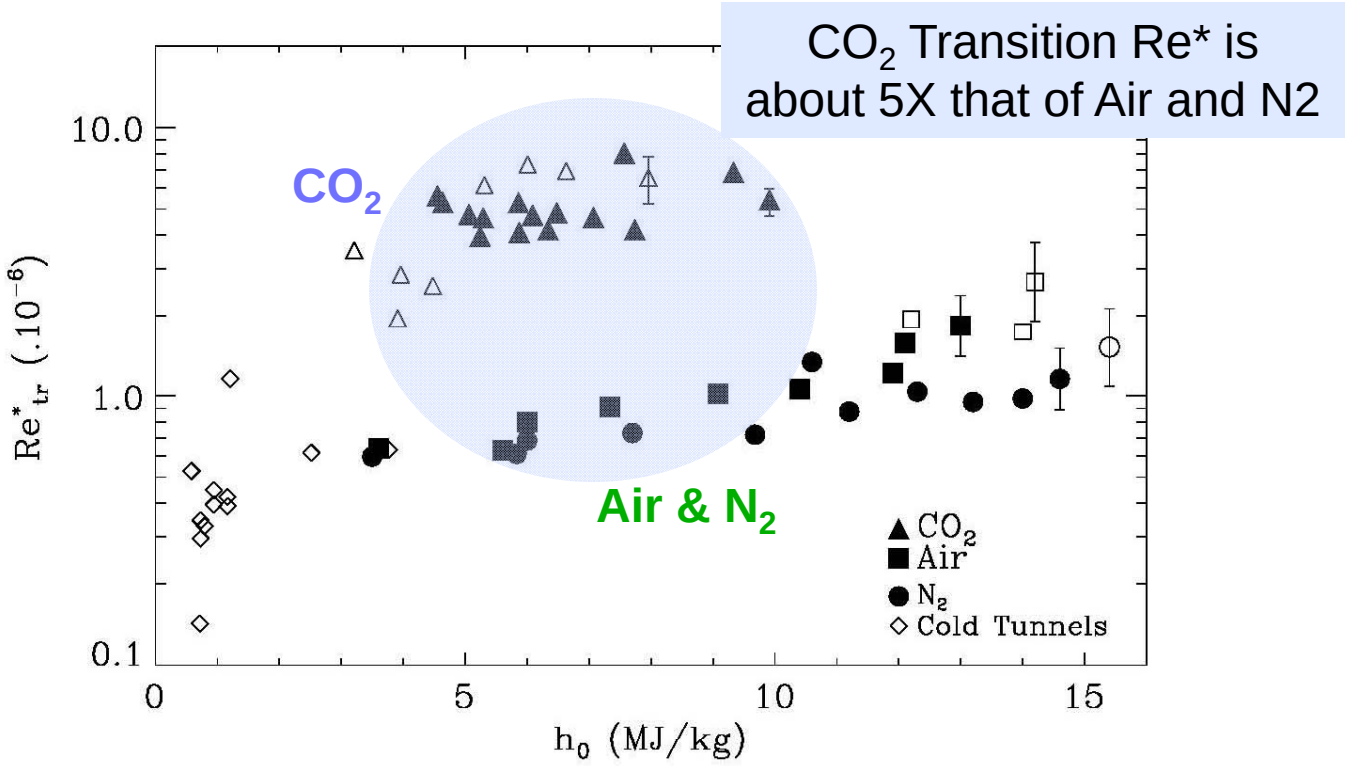

From Hornung, H.G., Adam, P.H., Germain, P., Fujii, K., Rasheed, A., "On transition and transition control in hypervelocity flows," *Proceedings of the Ninth Asian Congress of Fluid Mechanics*, 2002

Background

GALCIT
Caltech

Computations show that when pure CO_2 is in vibrational and chemical non-equilibrium, these relaxation processes absorb energy from acoustic disturbances in the boundary layer whose growth is responsible for transition in hypervelocity flows

Confirms trends seen in experiments where CO_2 exhibits delayed transition with respect to Air or N_2 for h_0~5-10MJ/kg

For air – no effect from vibrational relaxation and chemical reactions on stabilizing the boundary layer

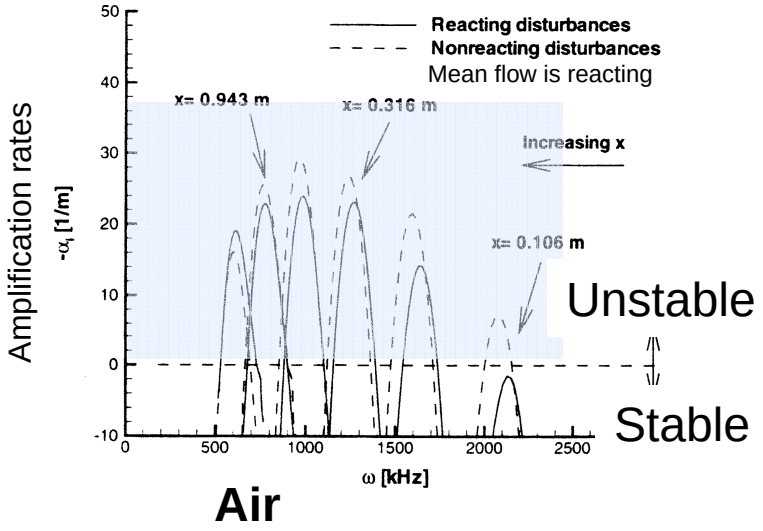

For CO_2 – vibrational relaxation and chemical reactions stabilizes the boundary layer

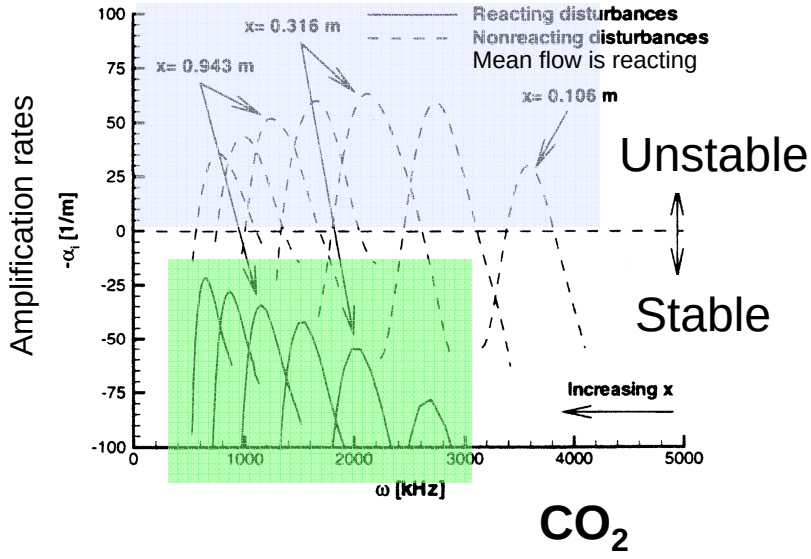

From Johnson, H.B., Seipp, T.G., Candler, G.V., "Numerical study of hypersonic reacting boundary layer transition on cones," *Physics of Fluids, 10 (10): 2676-2685 Oct. 1998.*

Background

GALCIT
Caltech

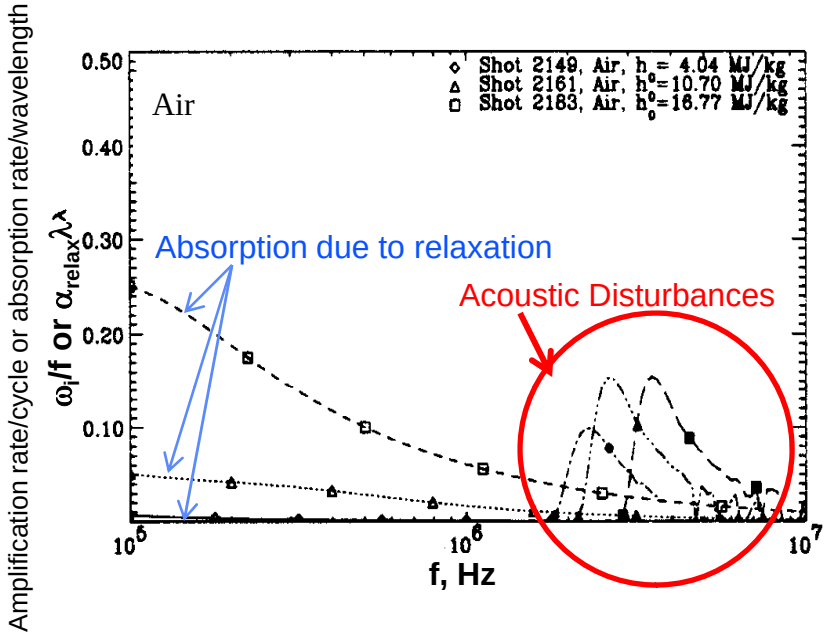

ir

Sound absorption rates peak much before the acoustic amplification rates become significant.

Expect no effect of the nonequilibrium processes in delaying transition in this case.

CO_2

- **Sound absorption rates and amplification rates for the acoustic disturbances peak in the range of interest (1-10 MHz).**
- **Expect a significant effect of the relaxation processes on acoustic damping.**

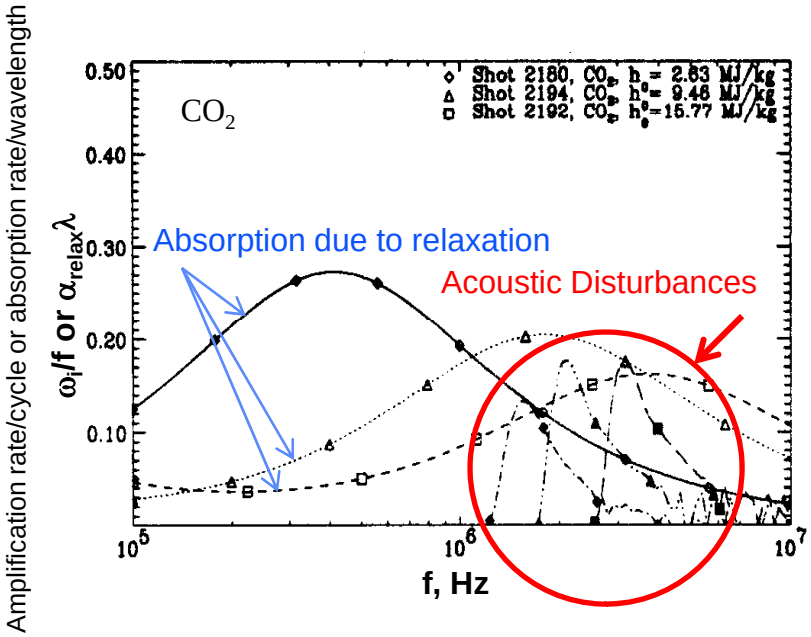

From Fujii, K., Hornung, H.G., "Experimental investigation of high-enthalpy effects on attachment-line boundary layer transition," *AIAA Journal, Vol. 41, No. 7, July 2003.*

Why vibration relaxation and dissociation damp acoustic waves

GALCIT
Caltech

- **Theory known for decades (Lighthill, 1956, Herzfeld and Litovitz, 1959, Clarke and McChesney, 1964, Vincentti and Kruger 1967)**

- **Following Clarke and McChesney, the linearization of perturbations of the N-S equations leads to damping curve as shown – Maximum damping occurs when $\omega\tau=a_f/a_e$**

- **Relaxation processes such as molecular vibration and dissociation cause damping of acoustic waves through *phase lag between pressure and density***

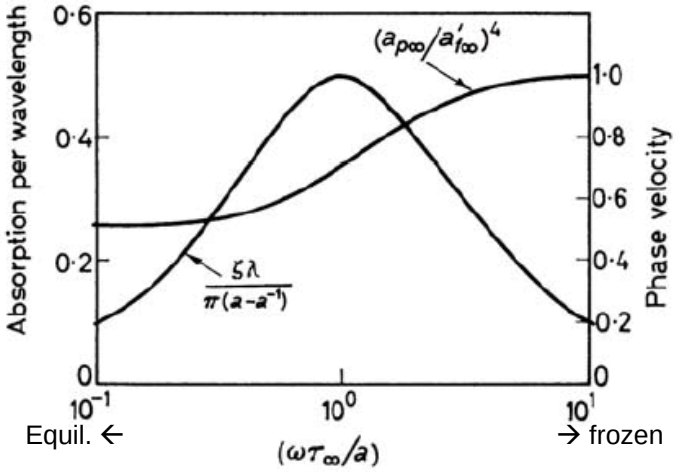

From Clarke and McChesney

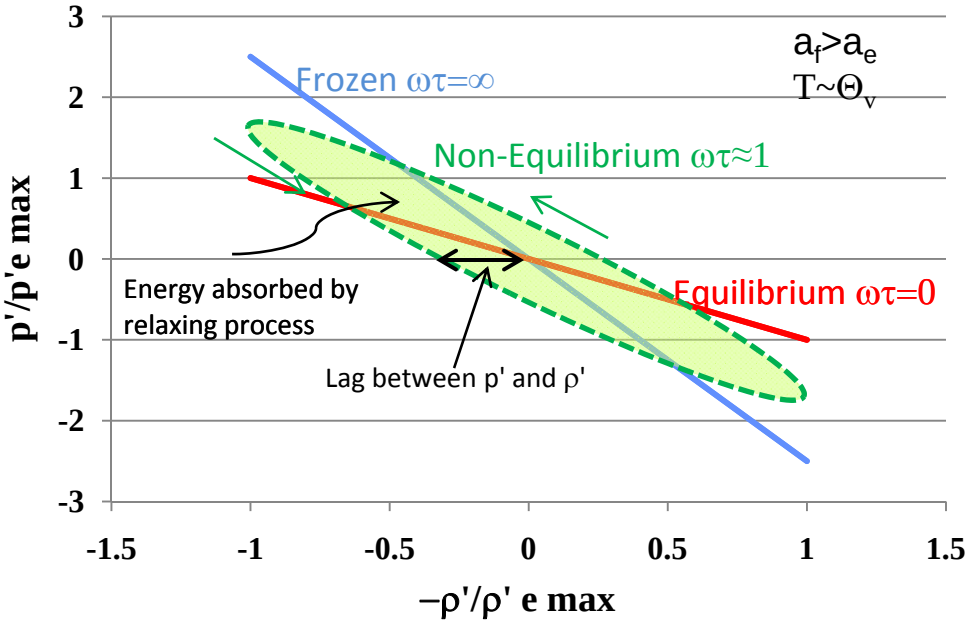

Experimental model and typical data

GALCIT
Caltech

Cone chosen because of wealth of data available for this geometry

Injector installed in a ~1m long 5-deg cone

72 holes,
0.51mm dia,
12 deg angle

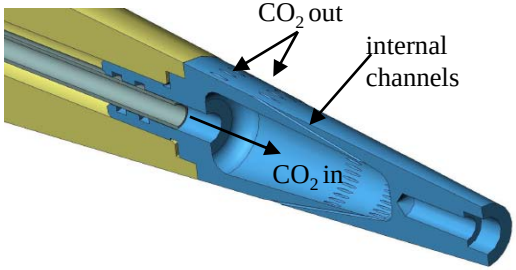

Sample heat transfer trace for CO_2 as a component in the free-stream test gas

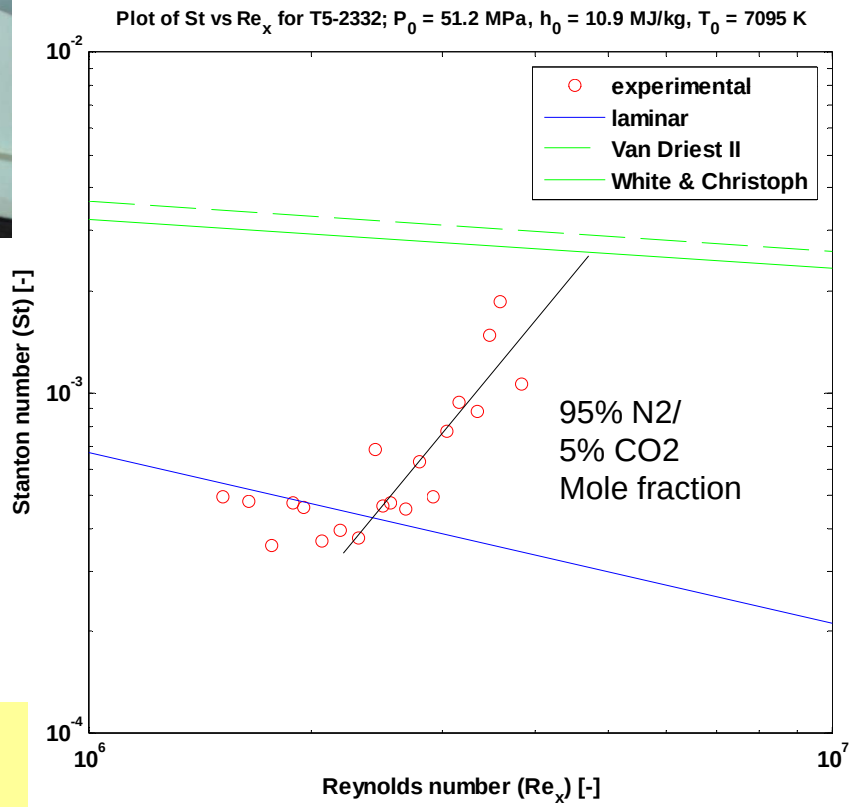

Transition determined from increase in heat flux

CO_2 as a component in the free-stream test gas

GALCIT
Caltech

- First step was to evaluate the impact of adding CO_2 to the free-stream
- This is to isolate the CO_2 effects from specific injector implementations
- Data shows that with 40% CO2 mole fraction Re*tr has about doubled from the baseline condition with 100% N2
- P_o~51 MPa, h_o~11 MJ/kg for N_2
- P_o~53 MPa, h_o~7.7 MJ/kg for Air

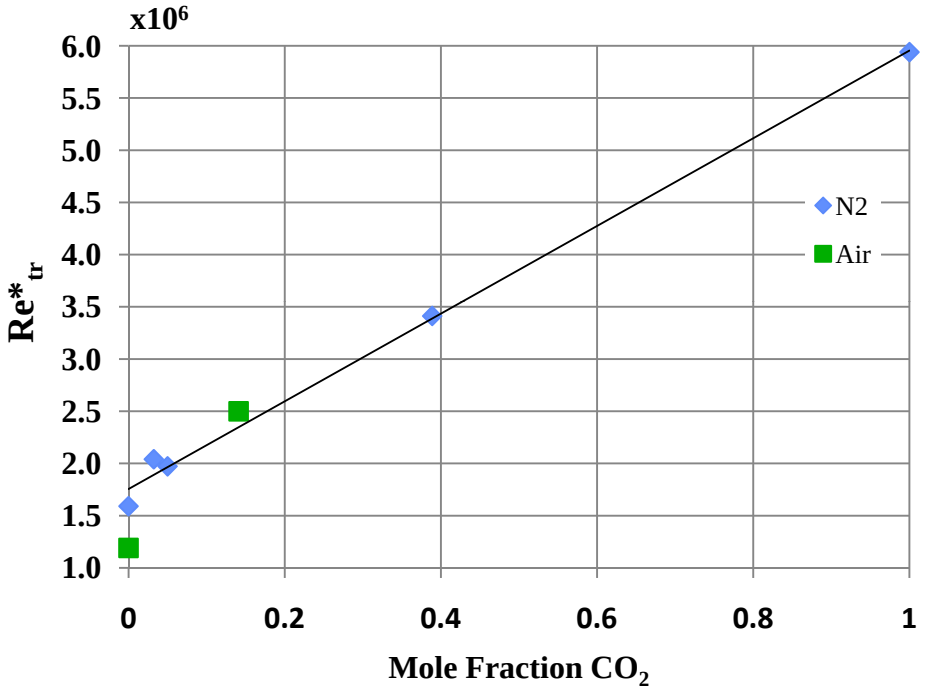

Preliminary data acquired with blends of CO_2/N_2 and CO_2/Air as the test gas shows effect of CO_2 to delay transition

CO_2/air mixtures in the free-stream

GALCIT
Caltech

100% air

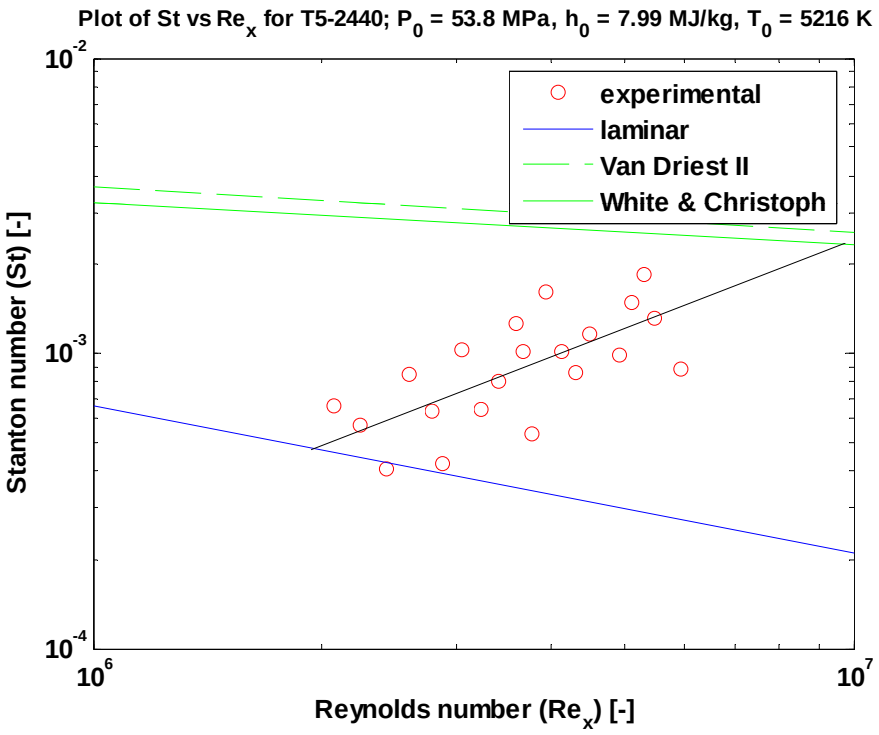

86% air /14% CO_2 mole fraction

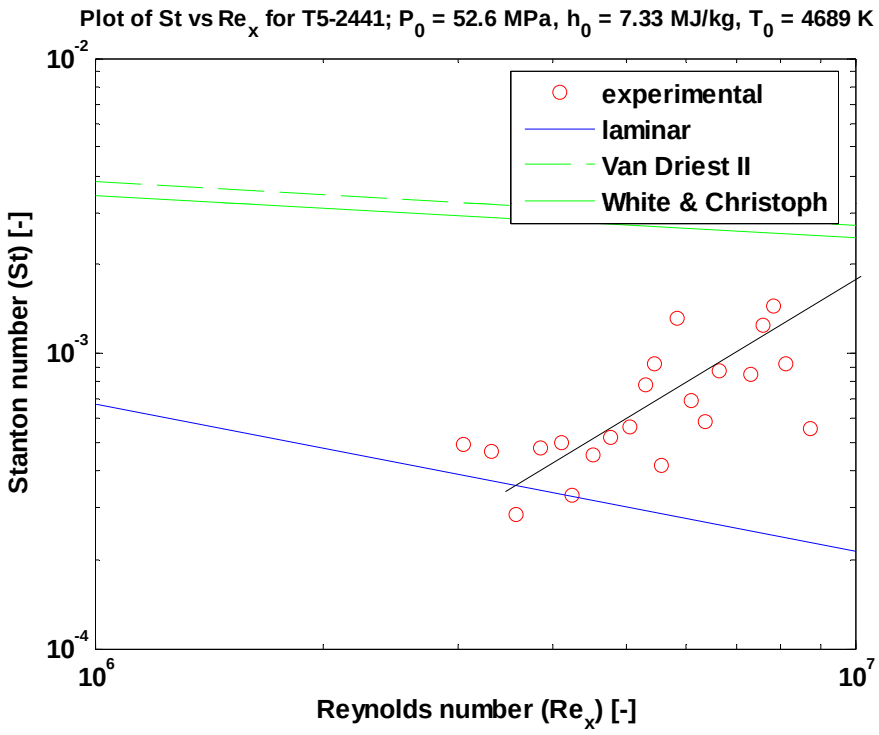

Preliminary data acquired with blends of CO_2/air as the test gas shows effect of CO_2 in delaying transition

CO_2 injection visualization

GALCIT
Caltech

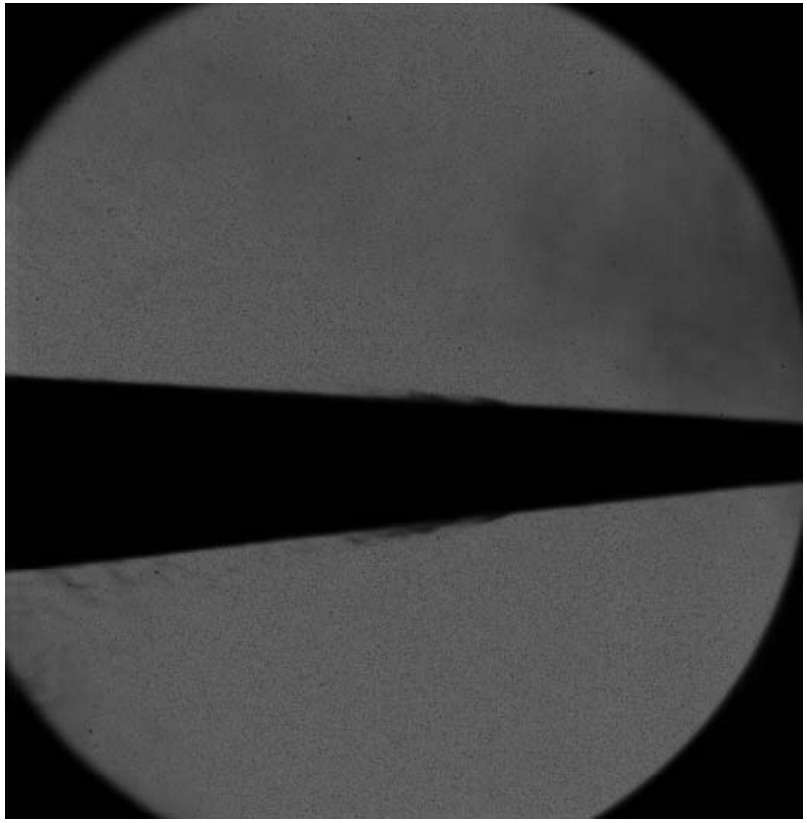

73 ms

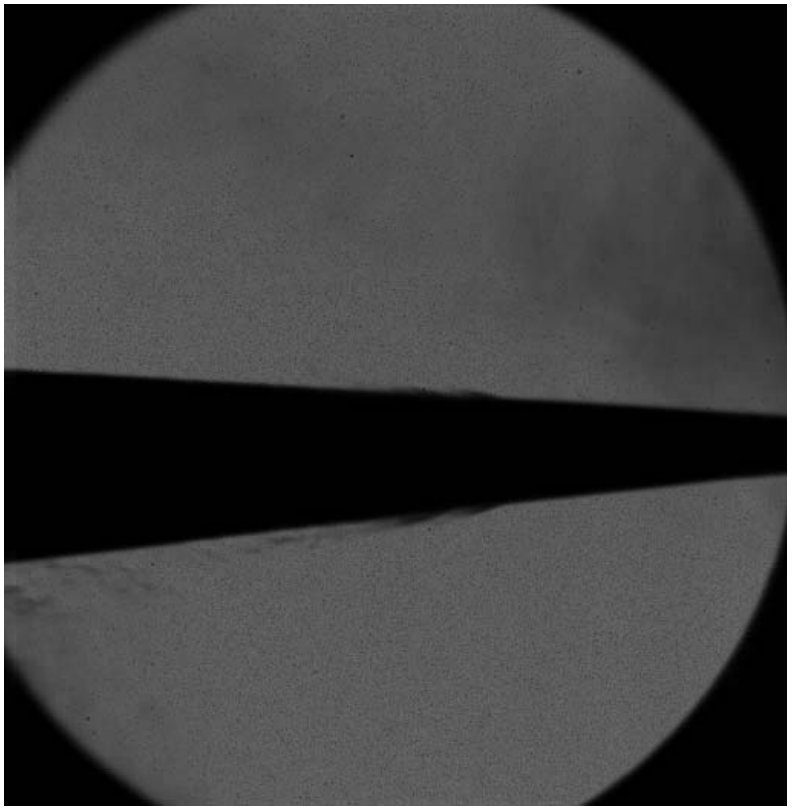

78 ms

Timing mechanism for CO_2 injection has been VALIDATED
Flow injection has been visualized

Mass flow calculations

GALCIT
Caltech

- **Mass flow determined from run tank pressure trace, $p_{rt}(t)$**
- **Injection system modeled as a series of straight pipes and expansions/contractions**
- **Obtain :**

$$\dot{m} = \alpha p_{rt}, \; p_{rt}(t) = p_{rt}(0)\exp(-\beta t)$$

where α and β are known.

- **For p_{rt}=300psi, $\dot{m} \approx 0.087$ kg/m^3 (mass flux in boundary layer 10cm from cone tip ~0.05 kg/m^3)**

Experimental and theoretical run tank traces

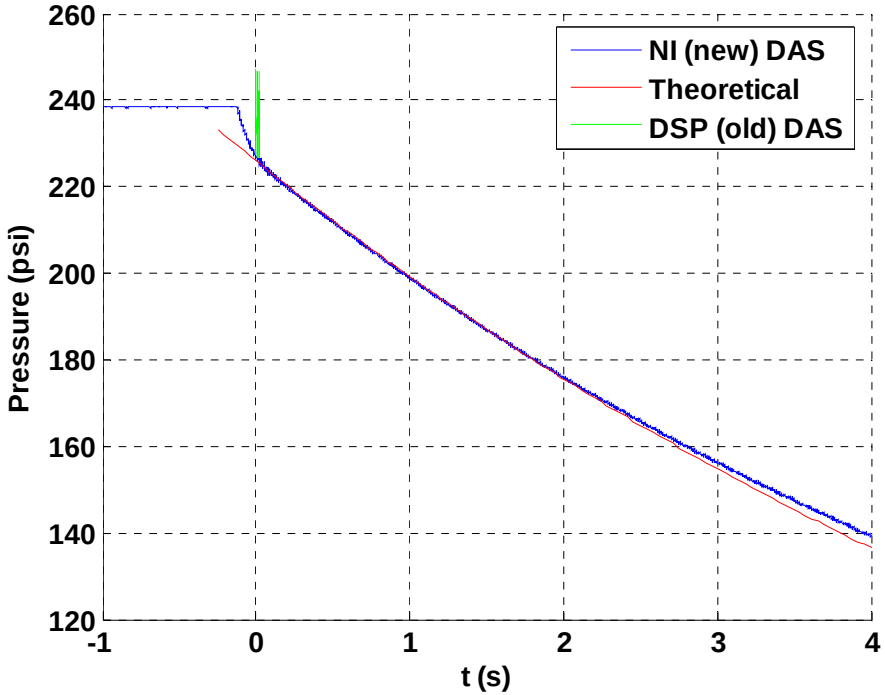

New Model

GALCIT
Caltech

80 thermocouples (vs 21 previously) - distributed uniformly in the axial and circumferential directions

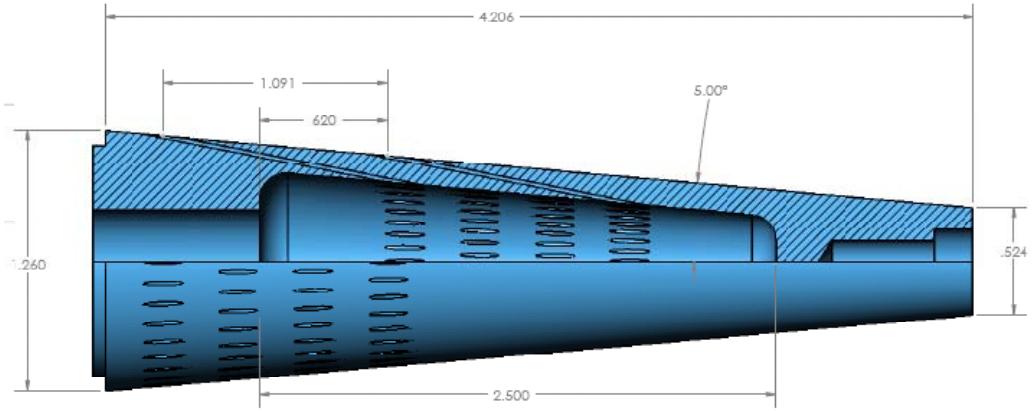

New injector tip – double the number of rows – larger flow area and greater mass flux for equal run tank pressures

Freestream conditions for CFD

GALCIT
Caltech

Stagnation Conditions		Freestream Conditions	
Pressure (MPa)	58.5	Density kg/m^3	0.06032
Temperature (K)	6305.3	Temperature (K)	1564
Enthalpy (MJ/kg)	10.47	Velocity (m/s)	4080
		Wall Temperature (K)	293
		Minf	5.1

Gas Composition (by mass fraction)	
N2	0.7345
O2	0.1844
NO	0.0654
N	0.0
O	0.0157

All at 300 K	Case 1	Case 2	Case 3
Pressure (psia)	32.2	64.4	107
Mass Flux (g/s)/hole	0.213	0.438	0.746

Numerical Grid

GALCIT
Caltech

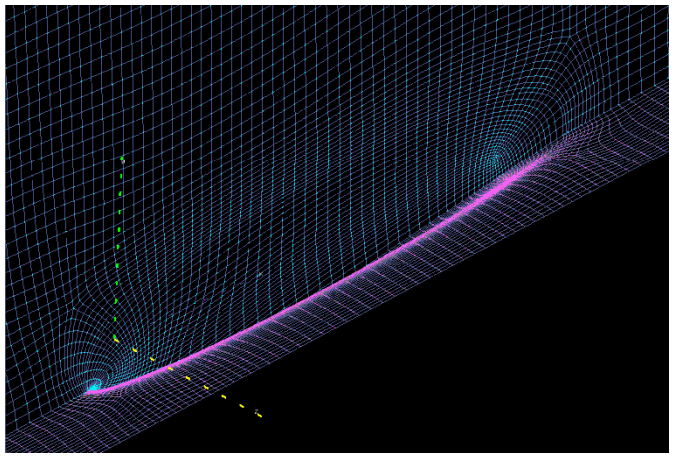

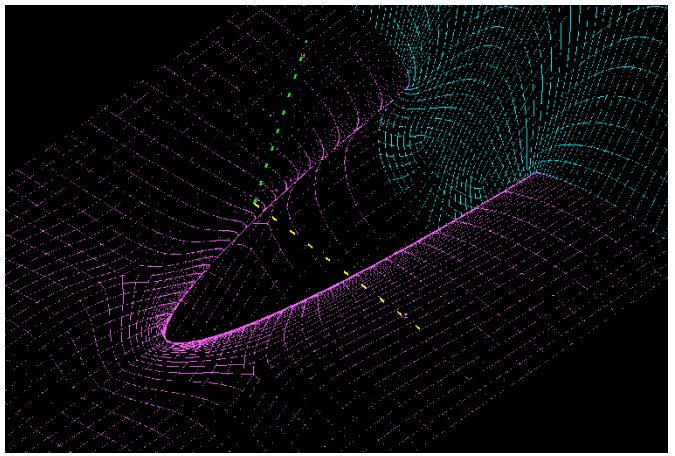

Injection Ports

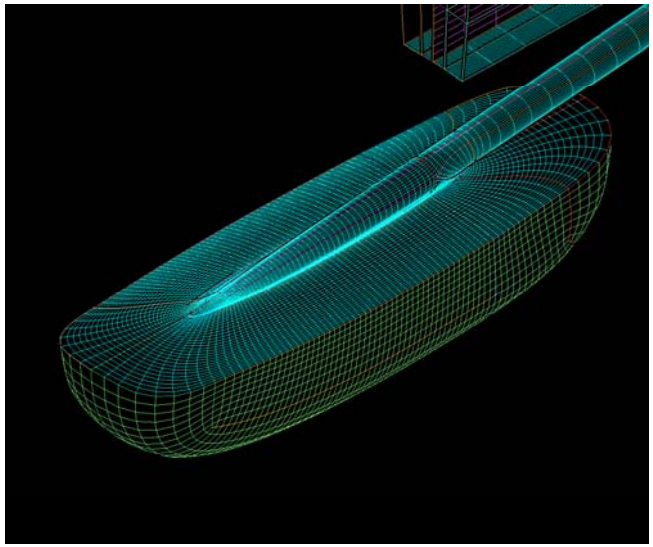

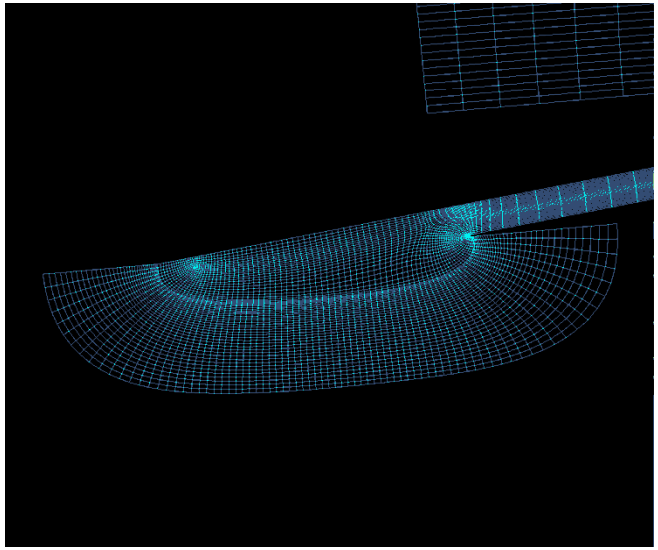

Reservoir

Mach Contours

GALCIT
Caltech

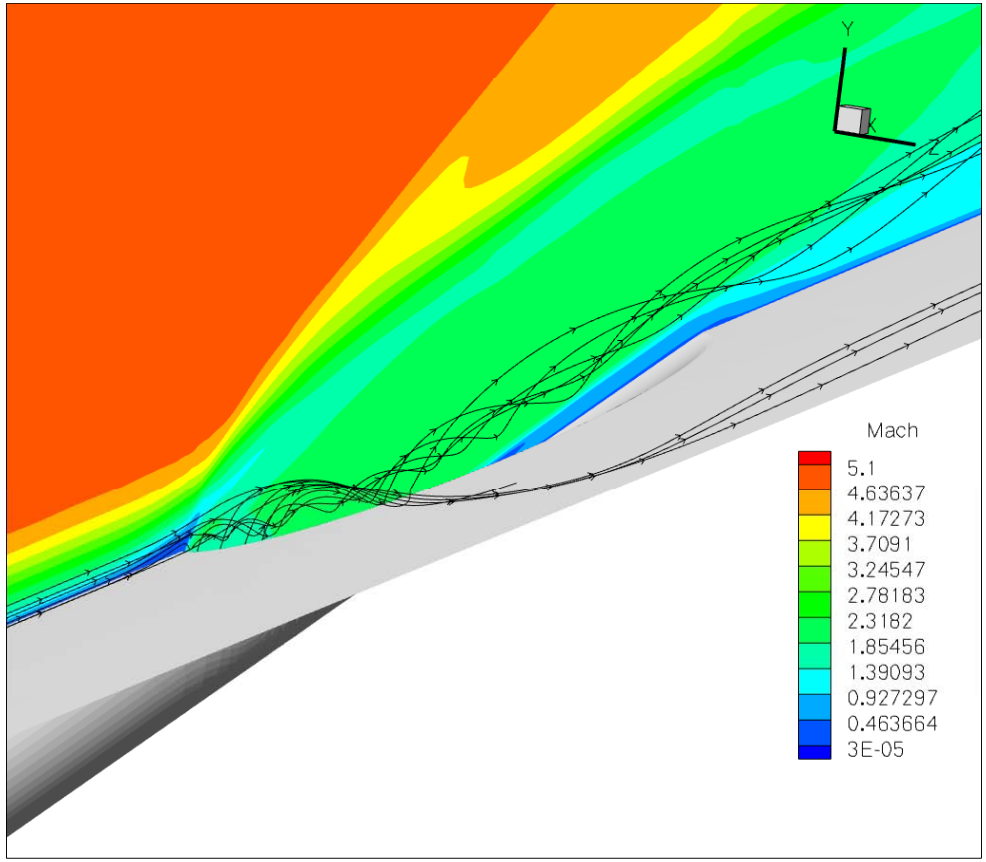

Case 1 - spanwise slices: axial distance of 0.3 m

GALCIT
Caltech

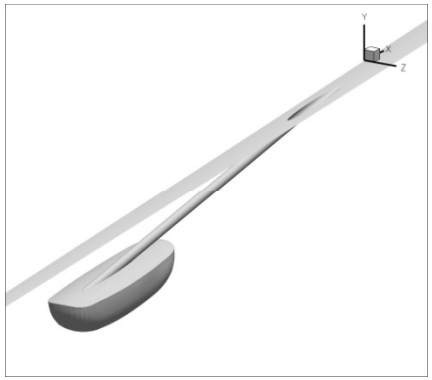

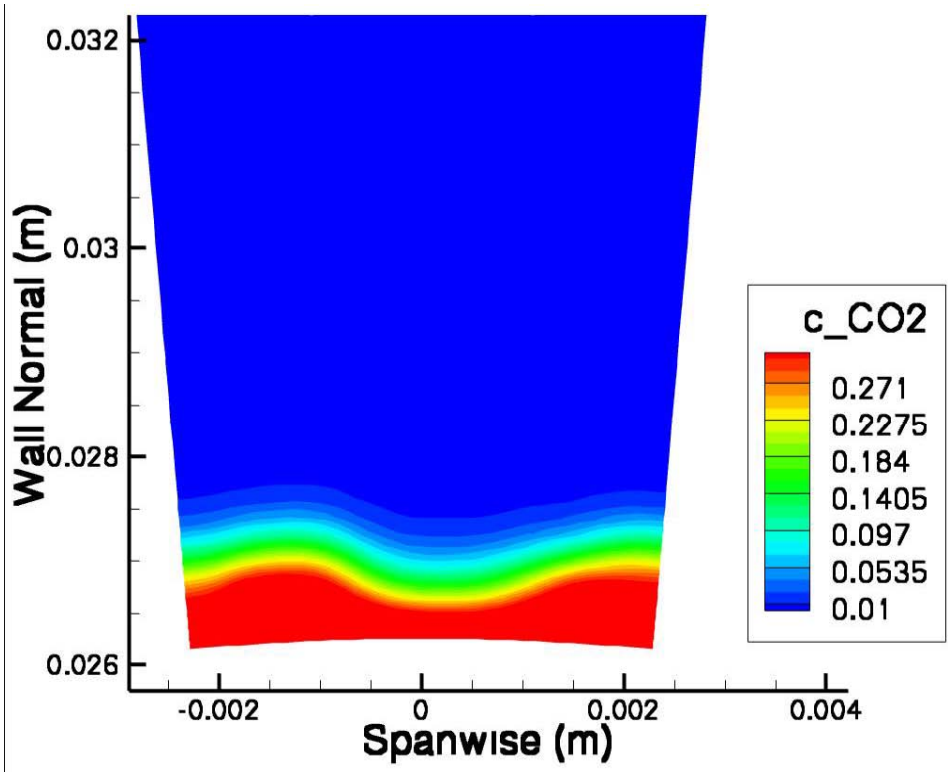

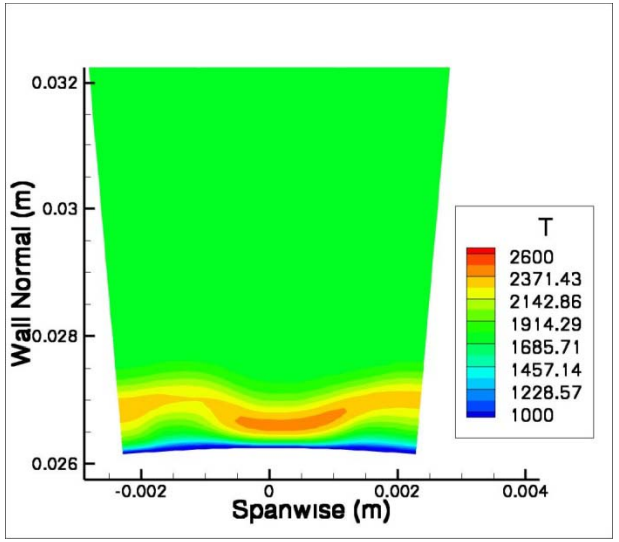

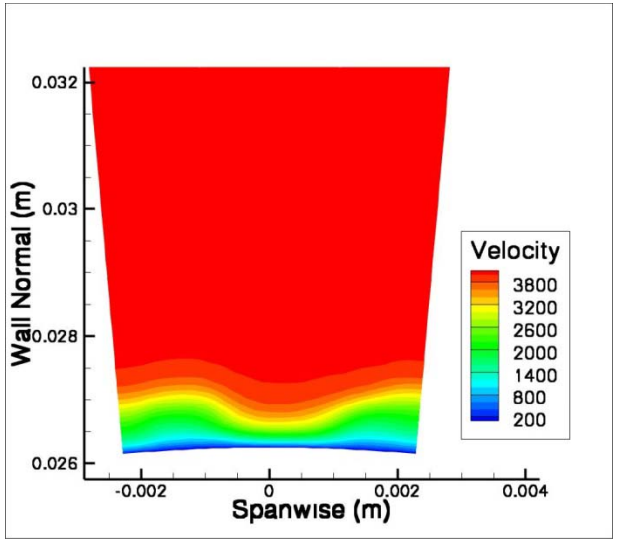

Case 1 - axial distance of 0.5m

GALCIT
Caltech

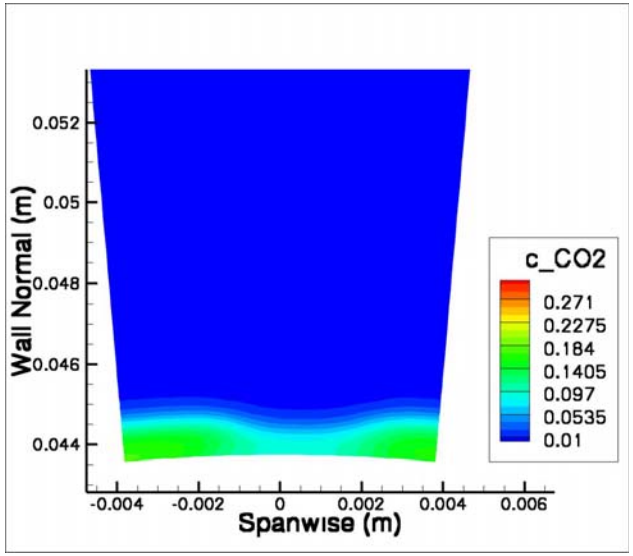

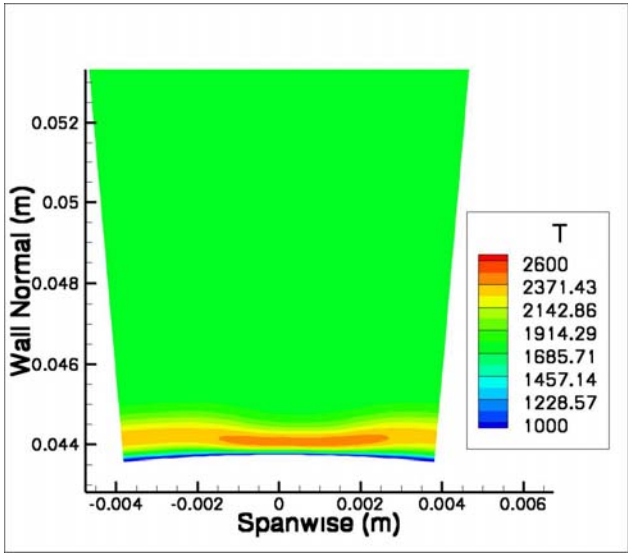

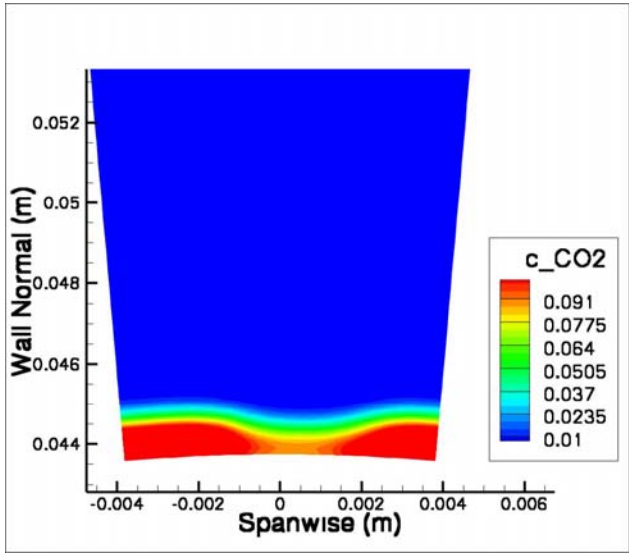

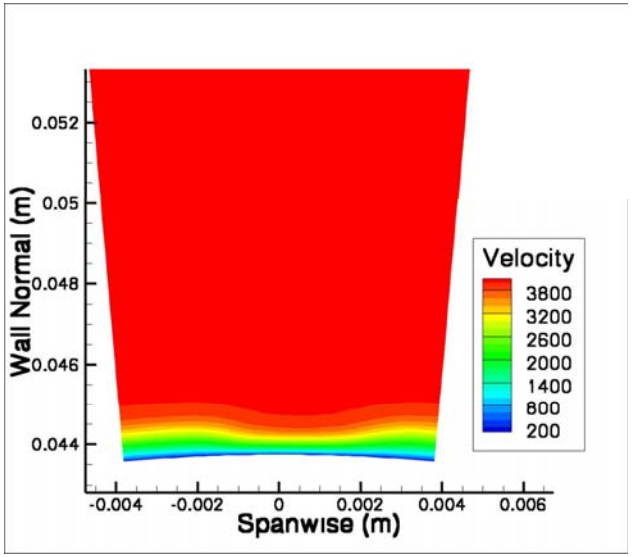

Conclusions

GALCIT
Caltech

- 100% CO_2 not needed to delay transition
  - For CO_2/N_2 test gas mixtures, increasing the CO_2 fraction increasingly delays the onset of transition.
    - For 40%CO_2/ 60%N_2 by mole fraction, Re*tr more than doubled in comparison to 100% N_2.
  - For CO_2/Air mixtures, delayed transition was also observed
- Timing for CO_2 injection system verified experimentally - about 100 ms buffer
- Verified experimentally a simplified model for calculating CO_2 mass flow rate
- New cone model has been built with approximately 4X as many thermocouples as before, uniformly distributed both axially and circumferentially
- New injection tip manufactured with approximately twice the injection area of the previous tip – larger flow rate for the same run tank pressure
- Numerical simulation of the injection flows
  - CO_2 heats up to more than 2000K within 20 cm from injection point – enough for vibration
  - CO_2 covers the entire surface of the cone at 20 cm from injection point – good mixing

Future Work

GALCIT
Caltech

- First test campaign with new cone
  - Run a baseline condition – 100% air to shake down new cone and verify transition location
  - Run with 4 values of the run tank pressure, all with new injector tip
  - Run with air as the injectant to compare with CO_2 results
  - Change the baseline condition if necessary
  - Test existing alternative injector tips
- Examine data and have a second test campaign guided by results obtained in first series
- Expand previously obtained data for air-CO_2 mixtures

Critical Challenges/Unsolved Problems

GALCIT
Caltech

- **Improve measurement accuracy**
  - **Previously used "recycled" cone whose thermocouples became faulty in the midst of testing**
  - **Redesigned and built new cone with 80 thermocouples**
    - **Same type of thermocouples as previously used in T5**
- **Injection technique**
  - **Heart of whether proposed technique is effective to delay transition depends on**
    - **Injecting at right location so that CO_2 reaches sufficiently high temperature for vibrational excitation**
    - **Injecting smoothly to avoid boundary layer tripping**
    - **Sufficient mass flow rate of injection while maintaining smooth flow, e. g. with transpiration injection**

Back up

First injector models

GALCIT
Caltech

Model No.	Hole diameter, d (mm)	No. Rows	Injection angle, α (deg)
1	0.51	2	12
2	0.76	1	11
3	0.76	1	12
4	1.02	1	11

Injector Variants

Model No. 1

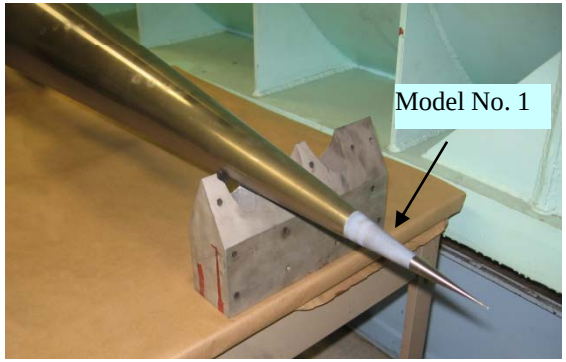

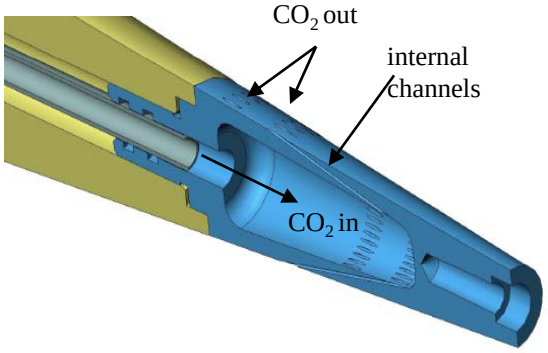

Model No. 2

Four injectors designed and built

Delay transition using non-equilibrium CO_2

GALCIT
Caltech

OBJECTIVE: Delay transition from laminar to turbulent flow in the boundary layer of a slender hypersonic body by injecting CO_2

PROBLEM: In hypersonic flight, heating loads are typically the dominant design factor

Turbulent heat transfer rates can be an order of magnitude higher than laminar rates at hypersonic Mach numbers

A reduction in heating loads means less thermal protection needed and hence less weight to carry, or conversely more payload deliverable for a given thrust.

A SOLUTION?

Transition in such flows occurs through the Mack mode – amplification of acoustic waves traveling in the boundary layer

Molecular vibration and dissociation damp acoustic waves

At relevant conditions, CO_2 absorbs most energy at the frequencies most strongly amplified by 2nd (Mack) mode

Inject CO_2 to delay transition in air flows of interest

CO_2 supply system

GALCIT
Caltech

The injection of CO_2 is triggered by the recoil of T5

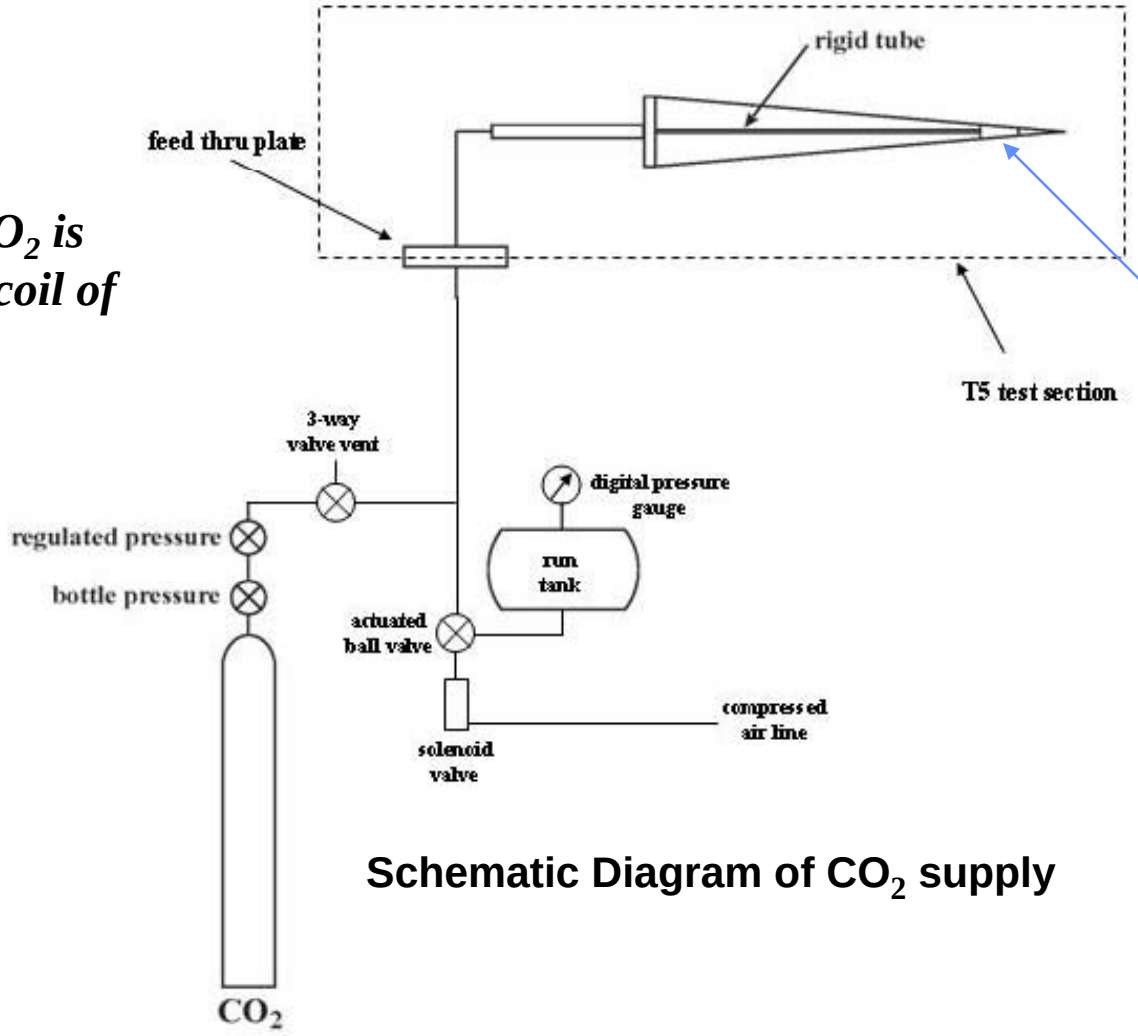

Schematic Diagram of CO_2 supply

Back-up charts

GALCIT
Caltech

REFERENCES

1. Hornung, H.G., Adam, P.H., Germain, P., Fujii, K., Rasheed, A., "On transition and transition control in hypervelocity flows," *Proceedings of the Ninth Asian Congress of Fluid Mechanics*
2. Fujii, K., Hornung, H.G., "Experimental investigation of high-enthalpy effects on attachment-line boundary layer transition," *AIAA Journal, Vol. 41, No. 7, July 2003.*
3. Johnson, H.B., Seipp, T.G., Candler, G.V., "Numerical study of hypersonic reacting boundary layer transition on cones," *Physics of Fluids, 10 (10): 2676-2685 Oct. 1998.*

CO_2 introduced in the free-stream test gas

GALCIT
Caltech

100% N2

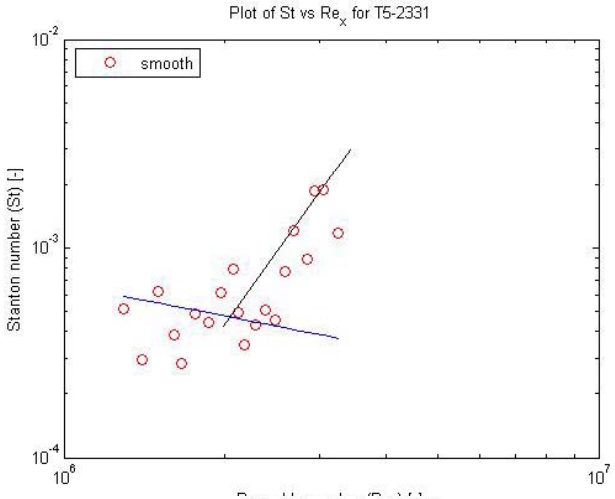

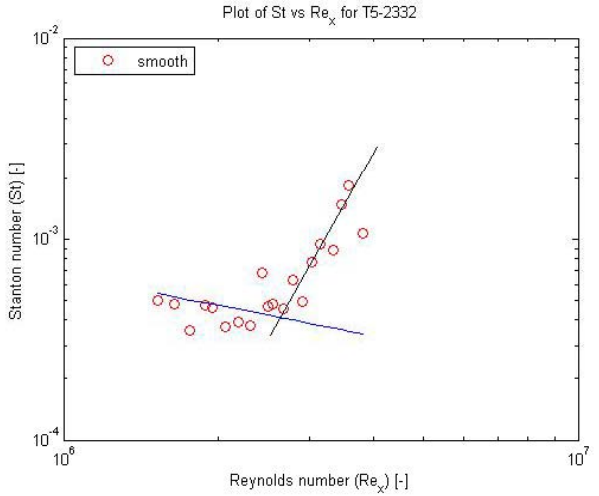

95% N2/
5% CO2

60% N2/
40% CO2

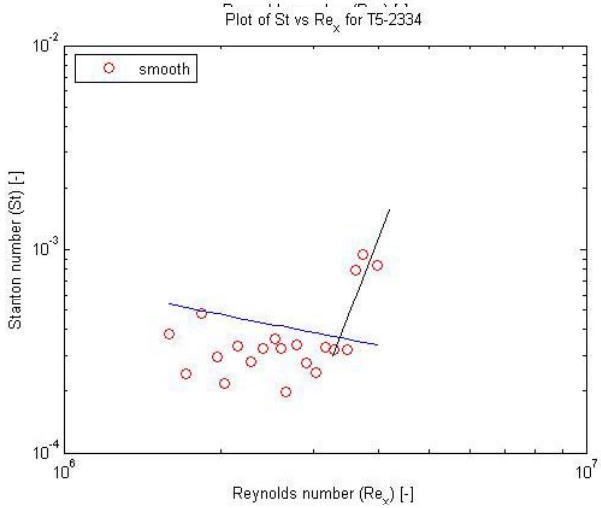

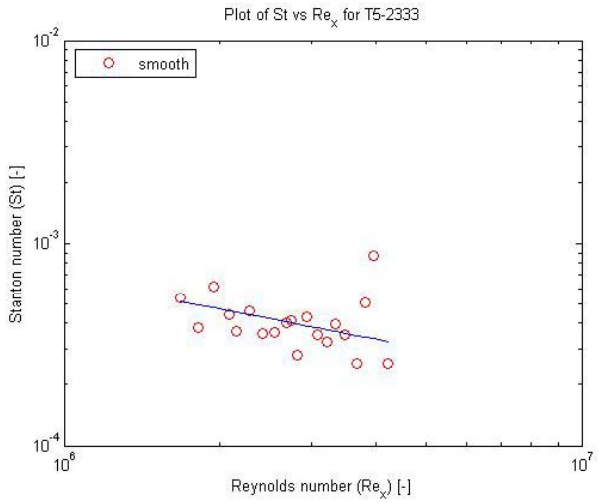

100% CO2

Experimental data shows effect of CO2 on delaying transition

CO_2 introduced to the boundary layer

GALCIT
Caltech

Typical profile for results with injection at the tip

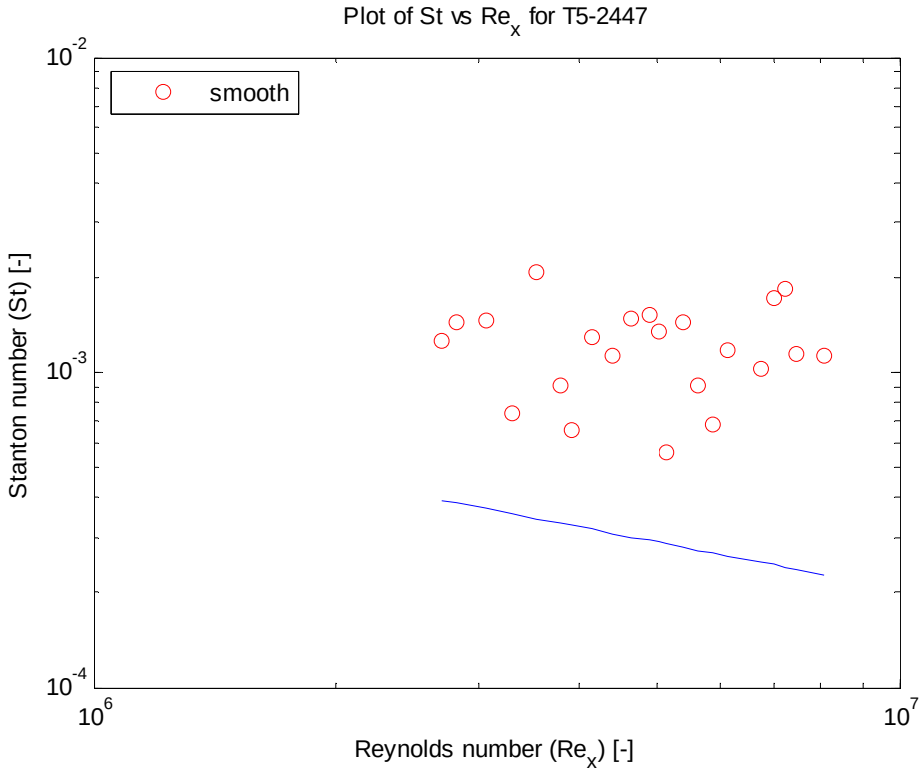

These results require further testing to confirm if the flow is transitional, laminar, or turbulent

Table A.1: Series 1 run conditions. Baseline and seeded flow.

Shot No.	P0	T0	h0	[N2]	[CO2]
	[MPa]	[K]	[MJ/kg]	[mol/mol]	[mol/mol]
2331	52.2	7375	10.75	1.0000	0.0000
2332	51.2	7095	10.90	0.9500	0.0500
2333	50.0	4434	9.43	0.0000	1.0000
2334	50.1	5380	10.89	0.6111	0.3889
2335	37.6	3459	5.58	0.0000	1.0000
2336	37.2	3606	6.12	0.0000	1.0000
2337	51.2	7379	11.37	0.9676	0.0324

Table A.2: Series 2 run conditions.

Shot No.	P0	T0	h0
	[MPa]	[K]	[MJ/kg]
2433	39.1	5305	8.34
2434	42.5	5538	8.87
2435	48.9	5843	9.53
2436	49.5	6069	10.07
2437	46.8	6567	11.33
2438	48.9	6069	10.08
2439	55.5	5715	9.15

Table A.3: Series 3 run conditions.

shot no.	P0	T0	h0	[air]	[CO2]
	[MPa]	[K]	[MJ/kg]	[g/g]	[g/g]
2440	53.8	5216	7.99	1.0000	0.0000
2441	52.6	4689	7.33	0.8000	0.2000
2442	53.3	4250	7.18	0.6000	0.4000
2443	53.9	3702	4.38	0.3000	0.7000
2444	53.0	3616	5.99	0.0000	1.0000
2445	53.3	3782	6.61	0.0000	1.0000

Table A.4: Series 4 run conditions. CO2 injection in high enthalpy air flow.

shot no.	P0	T0	h0	prt	$\dot{m}$
	[MPa]	[K]	[MJ/kg]	[MPa]	[kg/s]
2446	55.8	4742	6.85		
2447	50.5	4357	6.06	1.35	0.057
2448	48.4	4358	6.07	1.58	0.067
2449	45.7	4286	5.94	2.43	0.103

Delay transition using non-equilibrium CO_2

GALCIT
Caltech

OBJECTIVE

- **Combine the following facts to delay boundary layer transition from laminar to turbulent flow in slender hypersonic bodies using CO_2**
  - **Transition in this case happens through the second or Mack mode which can be approximated as acoustic waves traveling in the boundary layer**
  - **Molecular vibration and dissociation damp acoustic waves**
  - **CO_2 absorbs most energy at the frequencies most strongly amplified in a 2^{nd} mode transition**

WHY DELAY TRANSITION?

- **To reduce aerodynamic heating rates and drag on slender hypersonic vehicles**
  - **In a simple approximation, hypersonic aerodynamic heating grows as the cube of the free-stream velocity and linearly with free-stream density**
  - **Furthermore, turbulent heat transfer rates can be an order of magnitude higher than laminar rates for hypersonic Mach numbers**
  - **For high velocities heating loads become dominant in the design of a hypersonic vehicle**
- **A reduction in heating loads means less thermal protection needed and hence less weight to carry, or conversely more payload to deliver for a given thrust.**

Heating rates can be reduced by keeping the boundary layer laminar for longer lengths

Why delay transition?

GALCIT
Caltech

- **Reduction in aerodynamic heating rates and drag on slender hypersonic vehicles**
  - **In a simple approximation, hypersonic aerodynamic heating grows as the cube of the free-stream velocity and linearly with free-stream density**
  - **Furthermore, turbulent heat transfer rates can be an order of magnitude higher than laminar rates for hypersonic Mach numbers**
  - **For high velocities, the heating loads become dominant in the design of a hypersonic vehicle**
- **A reduction in heating loads means less thermal protection needed and hence less weight to carry, or conversely more payload to deliver for a given thrust.**
- **While one might not have control over the free-stream velocity, heating rates can be reduced by keeping the boundary layer laminar for longer lengths**

CO_2 introduced in the free-stream test gas

GALCIT
Caltech

Shot No.	P_0 (MPa)	T_0 (K)	h_0 (MJ/kg)	[N_2] or [air] (mol/mol)	[CO_2] (mol/mol)
2331	52.2	7375	10.75	1.00 N2	0.00
2332	51.2	7095	10.90	0.95 N2	0.05
2333	50.0	4434	9.43	0.00 N2	1.00
2334	50.1	5380	10.89	0.61 N2	0.39
2337	51.2	7379	11.37	0.97 N2	0.03
2440	7.99	53.8	5216	1.00 air	0.00
2441	52.6	4689	7.33	0.86 air	0.14

Experimental facility: T5, Caltech

GALCIT
Caltech

Injector installed in a ~1m long 5-deg cone to be tested in T5

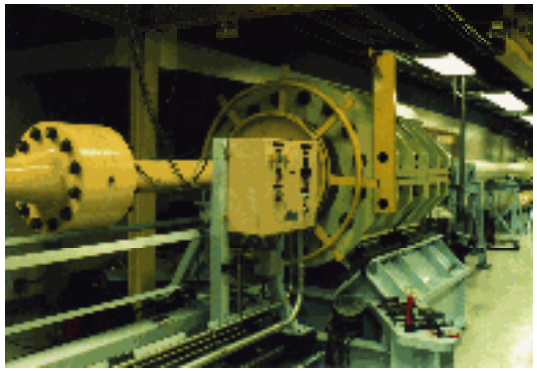

T5

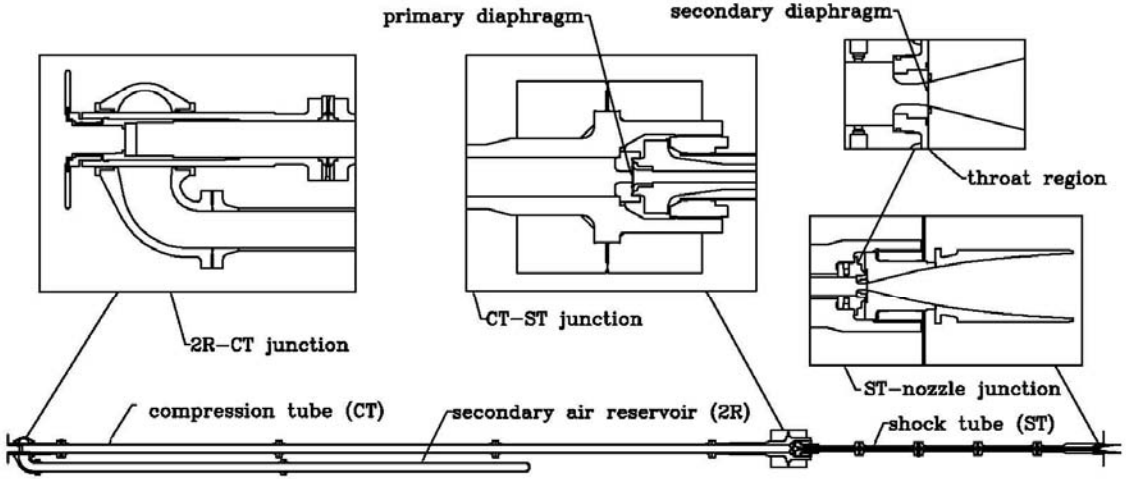

Schematic of T5

Vibrational temperatures

GALCIT
Caltech

species	M_w g/mol	$\sigma\Theta_{rot}$ K	h_f^o J/mol	g_v	Θ_v K	g_{e_o}	g_{e_i}	ϵ_e J/mol
N_2	28.016	5.79	0.0	1	3353.2	1	3	6.015×10^5
							6	7.136×10^5
							1	7.342×10^5
O_2	32.000	4.16	0.0	1	2239.0	3	2	9.225×10^4
							1	1.579×10^5
							3	4.320×10^5
							3	5.960×10^5
Ar	39.944	–	0.0	–	–	1	5	1.115×10^6
							3	1.122×10^6
N	14.008	–	4.713×10^5	–	–	4	6	2.301×10^5
							4	2.308×10^5
							6	3.452×10^5
							12	9.971×10^5
O	16.000	–	2.468×10^5	–	–	5	3	1.903×10^3
							1	2.717×10^3
							5	1.899×10^5
							1	4.044×10^5
							5	8.829×10^5
NO	30.008	2.45	8.990×10^4	1	2699.2	4	2	5.262×10^5
							4	5.496×10^5
C	12.011	–	7.116×10^5	–	–	1	3	1.962×10^2
							5	5.204×10^2
							5	1.219×10^5
							1	2.590×10^5
							5	4.036×10^5
CO_2	44.011	1.13	-3.933×10^5	2	960.1	1		
				1	1992.5			
				1	3380.2			
CO	28.011	2.78	-1.139×10^5	1	3082.0	1	6	5.824×10^5
							3	6.687×10^5
							6	7.453×10^5
							2	7.785×10^5
H_2	2.016	175.09	0.0	1	6100.0	1	1	1.097×10^6
							2	1.196×10^6
							3	1.352×10^6
H	1.008	–	2.110×10^5	–	–	1	3	9.839×10^5
							4	1.166×10^6
							5	1.230×10^6

Dissociation temperatures

GALCIT
Caltech

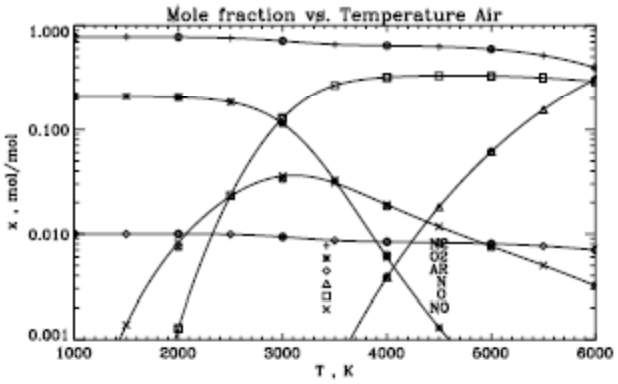

Air, $\rho = 0.01\mathrm{kg/m^3}$

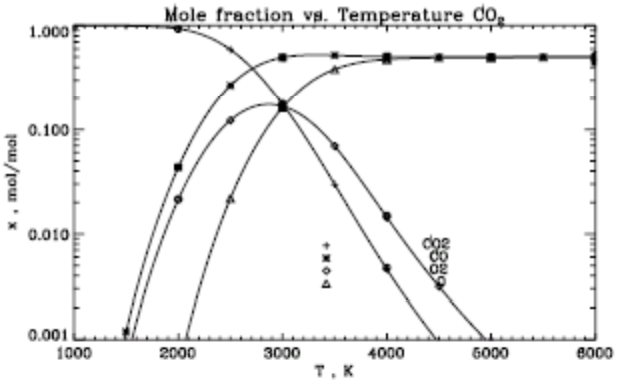

CO_2, $\rho = 0.01\mathrm{kg/m^3}$

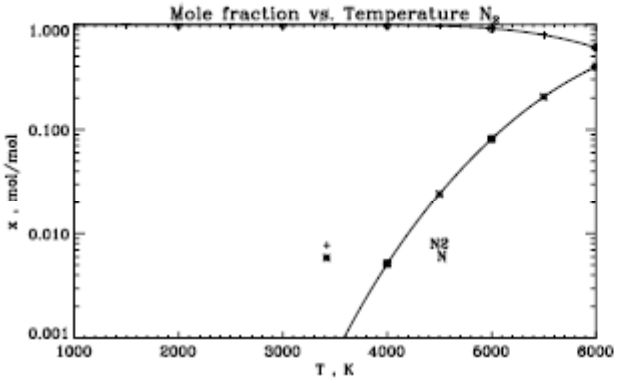

N_2, $\rho = 0.01\mathrm{kg/m^3}$

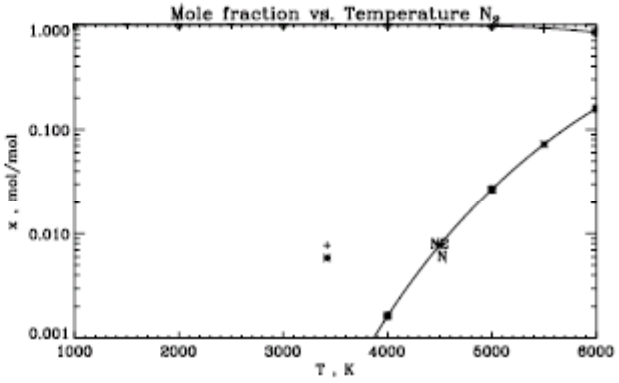

N_2, $\rho = 0.10\mathrm{kg/m^3}$

St=q/rhoe*ue*(h0-0.5*ue^2*(1-r)-CpTw)

Detailed data for conditions ran

GALCIT
Caltech

Table A.1: Summary of freestream conditions for all shots.

Shot	P_0 $[MPa]$	T_0 $[K]$	h_0 $[MJ/kg]$	P_∞ $[kPa]$	T_∞ $[K]$	ρ_∞ $[kg/m^3]$	U_∞ $[m/s]$	M_∞ $[-]$
2331	52.2	7375	10.75	21.8	1487	4.92×10^{-2}	4286	5.6
2332	51.2	7095	10.90	22.8	1569	4.96×10^{-2}	4211	5.4
2333	50.0	4434	9.43	40.9	2214	8.69×10^{-2}	3248	4.3
2334	50.1	5380	10.89	32.8	1980	6.29×10^{-2}	3799	4.7
2335	37.6	3459	5.58	27.7	1426	9.86×10^{-2}	2647	4.6
2336	37.2	3606	6.12	27.8	1532	9.12×10^{-2}	2741	4.6
2337	51.2	7379	11.37	23.2	1662	4.74×10^{-2}	4338	5.4
2433	39.1	5305	8.34	17.9	1250	5.00×10^{-2}	3712	5.4
2434	42.5	5538	8.87	20.3	1369	5.17×10^{-2}	3816	5.3
2435	48.9	5843	9.53	24.5	1522	5.60×10^{-2}	3942	5.2
2436	49.5	6069	10.07	25.7	1659	5.39×10^{-2}	4040	5.1
2437	46.8	6567	11.33	27.3	2178	4.37×10^{-2}	4363	4.8
2438	48.9	6069	10.08	25.5	1660	5.35×10^{-2}	4040	5.1
2439	55.5	5715	9.15	26.6	1423	6.51×10^{-2}	3873	5.3
2440	53.8	5216	7.99	25.1	1182	7.39×10^{-2}	3643	5.4
2441	52.6	4689	7.33	27.7	1285	8.05×10^{-2}	3407	5.1
2442	53.3	4250	7.18	33.0	1479	8.94×10^{-2}	3291	4.8
2443	53.9	3702	4.38	36.3	1448	1.13×10^{-1}	2938	4.7
2444	53.0	3616	5.99	40.3	1560	1.31×10^{-1}	2740	4.5
2445	53.3	3782	6.61	40.4	1674	1.21×10^{-1}	2834	4.5
2446	55.8	4742	6.85	22.4	931	8.36×10^{-2}	3384	5.7
2447	50.5	4357	6.06	18.9	783	8.43×10^{-2}	3193	5.8
2448	48.4	4358	6.07	18.0	783	8.01×10^{-2}	3193	5.8
2449	45.7	4286	5.94	17.1	762	7.84×10^{-2}	3164	5.8